Journal of Intelligent & Robotic Systems (2026) 112:41
https://doi.org/10.1007/s10846-026-02390-0

REGULAR PAPER

Static and Dynamic Friction Models for Robotic Manipulators: State of the Art and Experimental Comparison

Giuliano Fabris[1] · Lorenzo Scalera[1] · Paolo Boscariol[2] · Alessandro Gasparetto[1]

Received: 3 September 2024 / Accepted: 12 March 2026

Abstract
Achieving an accurate and efficient dynamic modelling is fundamental in many robotic applications. The effect of friction in the dynamic behaviour of a robot is one of the most challenging factors to predict, due to the complexity of the several phenomena that cause it. Several friction models are available in the literature, each of which can be more or less suitable depending on the situation and working conditions. In this paper, we present the state of the art and experimental comparison of friction models for robotic manipulators. We first consider both static and dynamic friction formulations to evaluate their ability to consider the different friction effects and the factors that influence friction behaviour. Then, twenty-five selected models are experimentally compared to evaluate their ability to predict friction effects in a UR5e robot with six degrees of freedom. The results of extensive experiments show good performance of most of the considered friction models in predicting the friction torque, and in evaluating the energy consumption of the robot when applied together a complete dynamic formulation. The findings of this study can be used as guidelines for determining the best friction model for the operating conditions under consideration.

Keywords Dynamics · Energy consumption · Friction modelling · Identification

1 Introduction

Accurate and efficient dynamic modelling of robotic systems is crucial for achieving satisfactory performances in many applications. Examples are the design of control algorithms [1], where a precise torque prediction is needed to ensure good trajectory tracking performance [2], or the execution of industrial manufacturing operations like robotic milling, which requires the knowledge of the dynamic model of the robot to avoid undesired vibrations [3]. Moreover, dynamic modelling of robotic systems has application in human-robot interaction [4], and collision detection [5], considering for example that a collision can be detected if the actual torques deviate from those computed with the robot dynamic model [6].

Developing a reliable dynamic model is fundamental also for energy efficiency purposes, since it is the basis of different methods for reducing the energy expenditure of a robotic or mechatronic system. Examples of energy efficiency approaches that rely on the dynamic modelling are the optimal task placement [7, 8], the exploitation of the system natural motion [9], and the trajectory planning [10, 11]. Particularly, optimizing robot trajectories requires a good dynamic model for a precise computation of motor torques and energy consumption, in order to find the optimal combination of the trajectory variables [12].

The dynamics of a robotic system is influenced by inertial (masses, centers of mass, and moments of inertia) and friction parameters, which are often challenging to be correctly identified. The nonlinear phenomenon of friction is omnipresent in mechanical systems, and depends on contact geometry and surfaces, topology, properties of the materials, relative velocity, lubricant, humidity, and temperature [13]. Friction results

✉ Lorenzo Scalera
lorenzo.scalera@uniud.it

Giuliano Fabris
giuliano.fabris@uniud.it

Paolo Boscariol
paolo.boscariol@unipd.it

Alessandro Gasparetto
alessandro.gasparetto@uniud.it

[1] Polytechnic Department of Engineering and Architecture, University of Udine, 33100 Udine, Italy

[2] Department of Industrial Systems Technology and Management, University of Padova, 36100 Vicenza, Italy

in energy losses and heating of the contact surfaces. Focusing on robotics, friction introduces nonlinearities that can lead to motion control issues, including trajectory tracking errors, limit cycles, and dynamic instabilities (e.g., stick-slip can cause abrupt accelerations at low velocities) [14]. Due to its complexity and impact on the dynamics of a mechanical system, friction is one of the most important and undesired phenomena to be considered in order to develop a reliable dynamic model of a robotic system [15].

Nowadays, an accurate friction modelling is fundamental in modern manufacturing scenarios like collaborative robotics, where lightweight robots that work at limited power and speed are often used [16]. Robotic manipulators for collaborative robotics applications generally employ brushless motors of reduced size and strain wave gearing, like harmonic drives. Harmonic drives are composed of three main elements: an elliptical disk (wave generator) that is connected to the motor shaft and acts as input; a deformable cylindrical cup with external teeth (called flexspline) which acts as output; and a fixed ring with internal gearing (circular spline) that surrounds the other two components and meshes with the flexspline. Harmonic drives are considered the primary sources of friction losses in a robot joint, as friction is generally relatively minimal for brushless motors [17]. This type of transmission is largely adopted since it presents a favorable power density and high gear ratio in a single stage, resulting in a compact size and low weight. However, the mechanical efficiency of harmonic drives is limited, primarily due to meshing losses between the flexspline and the circular spline. The flexspline has less teeth than the circular spline, characteristic that allows to obtain, during the rotation of the wave generator, a relative motion between the flexspline and the circular spline, but that leads to resistant friction forces [18]. Furthermore, the complex nonlinear friction and hysteresis characteristics of these transmissions make their accurate mathematical modelling challenging [19].

Dynamic and friction modelling for collaborative robotics has been widely investigated and different models have been proposed in the literature. For instance, Raviola et al. [20] studied the influence of the temperature and the mounting configuration on the dynamic behaviour of the UR3 and UR5 robots with six degrees of freedom (DOFs), whereas the authors in [21] modeled the effects of the temperature and the load torque on the friction torque in a 6-DOF ABB IRB 6620 robot. Moreover, Gaz et al. [22] identified the dynamic parameters of a UR5 e-series robot for human-robot interaction. The dynamic and friction modelling of other robots for collaborative robotics applications have been studied, such as the 7-DOF Franka Emika Panda arm [23, 24], the 6-DOF Indy7 robot [25, 26], the 6-DOF KUKA KR10 robot [27], and the 6-DOF COMAU Racer 7 robot [28]. However, in all the above mentioned works, the friction behaviour is described using only one friction model at a time, without highlighting advantages and disadvantages of different friction formulations. To the best of our knowledge, a comparison of several static and dynamic friction models supported by an extensive experimental validation is not present in the current literature.

In this paper, we present the state of the art on static and dynamic friction models for robotic manipulators, and an experimental comparison of twenty-five selected friction formulations on a UR5e robot by Universal Robots. The static friction models consider only the current state of the system and adopt different mathematical functions to capture friction effects at low velocity. Models where friction is only function of velocity, and models that take into account also the effects of joint temperature and load torque are both considered in this work. Differently, dynamic friction models account for the history of the system in the friction definition by means of a differential formulation. Friction models based on artificial neural networks are not considered in this work. The considered friction models are applied to a UR5e robot to evaluate the friction effects in different working conditions. We take into account not only the influence of velocity (in both the full velocity range of the robot and at low velocities only), but also the history of the system, and changes in the joint temperature and the load torque.

This paper is an extended version of our previous work in [29]. With respect to [29], this work includes novel contributions that allow us to: (i) compare additional static friction models that describe friction effects in alternative ways or consider other friction dependencies (e.g., the power flow direction) and evaluate the friction models capability to approximate experimental data in extensive experimental tests on a UR5e arm; (ii) consider the thermal and dynamic effects in the friction behaviour; (iii) evaluate the performance not only of static but also of dynamic friction models.

To summarize, the main contributions of this work are:

- a comprehensive state of the art on static and dynamic friction models for robotic manipulators, with particular focus on industrial robots used in collaborative robotics;
- an extensive experimental comparison of twenty-five selected static and dynamic friction models applied to a UR5e robot with six degrees of freedom;
- a quantitative evaluation of the friction prediction capabilities of the considered friction models in terms of: (i) joint friction torques in a wide range of joint velocities; (ii) energy consumption of the robot when each friction model is included in the whole dynamic model of the robot; (iii) modelling the effects of temperature and load torque on friction behaviour.

The paper is organized as follows: Section 2 describes the state of the art on static (Section 2.1) and dynamic

(Section 2.2) friction models for robotic manipulators. Section 3 illustrates the friction parameters identification, whereas Section 4 the experimental setup. The experimental results and the comparison of the considered friction models are reported in Section 5, and the discussion in Section 6. Finally, Section 7 outlines the conclusions and the future developments of this work.

2 Friction Modelling

Friction modelling is crucial in mechatronic and robotic systems, in which robot joints operate under various motion regimes depending on the required application. Numerous friction models can be found in the literature, each with a different degree of complexity and effectiveness in capturing the diverse phenomena associated with friction. The major friction contributions that are usually considered are the Coulomb friction, the viscous friction, and the Stribeck effect [30] (Fig. 1). The Coulomb friction is the constant torque that opposes to the motion, whereas the viscous friction is proportional to velocity. Furthermore, the Stribeck effect considers the transition between Coulomb and viscous friction at low velocities. In this phase, the friction torque initially decreases with velocity, until a minimum value (i.e., Stribeck velocity [21]); then, the friction torque increases with velocity.

As mentioned above, friction models can be classified in static and dynamic models [31]. Static models have in general a simpler structure and depend on a lower number of parameters with respect to dynamic models. Dynamic models are generally based on a differential formulation, enable to take into account friction behaviour at rest state, as well as at both low and high velocities [32]. These two classes of models also differ in the way they describe friction effects close to zero velocity. For their different characteristics, static and dynamic models are suitable for different operating conditions. In the following, an overview on the state of the art of these two classes of friction models for robotic systems available in the literature is presented, analyzing their mathematical formulation, as well as the considered friction effects.

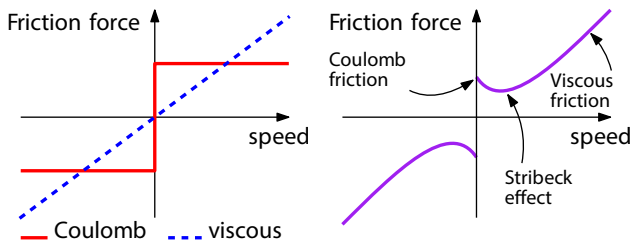

Fig. 1 Graphical representation of major friction contributions

2.1 Static Friction Models

Static models take into account the current state of the system and not its history, generally only considering the dependence of friction on velocity. Therefore, they are more suitable for applications with significant relative velocities between the contact surfaces and limited transitions at velocities close to zero [32]. In the following, we provide an overview on the main static friction models, with particular focus on those used in the contexts of industrial and collaborative robotics. The complete formulations of the models that are experimentally compared on the UR5e robot (Section 5.1) are reported and described in Tables 1, and 2. In the tables, the terms a_k indicate the friction parameters that have to be optimized in order to fit each model with the experimental data from the robot. Moreover, $\boldsymbol{\tau}_{f,th}$ represents the theoretical friction torque computed by the model, $\dot{\boldsymbol{q}}$ is the vector of the joint velocities, $\boldsymbol{T}$ indicates the vector of the joint temperatures, and $\boldsymbol{\tau}_l$ represents the load torques.

The most well-known static model is the one proposed by Coulomb [33] in 1773, which is adopted when a simple and computationally efficient formulation of friction effects is required, as in [24, 34]. In the original Coulomb model, the friction torque is considered as a term dependent on the direction of the velocity. Although the Coulomb formulation is effective in describing the behaviour of friction in many situations, it is not able to correctly reproduce friction effects at low velocities. This is due to the discontinuity at zero velocity, caused by the *sign* function (see the model formulation in Table 1), which is not realistic. In the following, we refer to the Coulomb and viscous friction model as just Coulomb model, since the viscous term is present in most friction formulations.

Alternative models include additional terms to account for friction effects at low speed. For instance, Grotjahn et al. [35] added to the Coulomb model a term proportional to the cubic root of the velocity (Grotjahn (A)), or a term proportional to the arctangent (*arctan*) of the velocity (Grotjahn (B)). These friction formulations have been used to model friction in a 6-DOF Siemens Manutec-r15 robot. Bittencourt and Gunnarsson [21] modeled the Stribeck effect in the joints of a 6-DOF ABB IRB 6620 robot with a decreasing exponential function (Bittencourt (A)), whereas Dong et al. [36] proposed to use two different decreasing exponential terms in the friction model of a 6-DOF Stäubli TX-90 robot. Moreover, Karahan and Karci [37] modeled the Stribeck effect with a decreasing exponential function, and each of the friction parameter is defined for four different working conditions, depending on the signs of velocity and acceleration.

Differently, Hao et al. [38] generalized the Coulomb model adopting a third-degree polynomial formulation (Hao (A)), which has been used to model friction in a 6-DOF EFORT ER3A-C60 robot. Moreover, Wolf and Iskandar [39]

Table 1 Overview on the static friction models (accounting for joint velocity only) considered in this paper

Friction model	Year	Ref.	Formulation	Description
Bittencourt (A)	2012	[21]	$\boldsymbol{\tau}_{f,th} = \left(a_1 + a_2 e^{-\lvert \frac{\dot{\boldsymbol{q}}}{a_3} \rvert^{a_4}}\right)\text{sign}(\dot{\boldsymbol{q}}) + a_5\dot{\boldsymbol{q}}$	• constant directional term • decreasing exponential term • velocity-proportional term
Clochiatti	2024	[44]	$\boldsymbol{\tau}_{f,th} = a_1\dot{\boldsymbol{q}} + a_2 \tanh\left(\frac{\dot{\boldsymbol{q}}_{dir}}{\epsilon}\right) + a_3 \tanh\left(\frac{\dot{\boldsymbol{q}}_{rev}}{\epsilon}\right)$ with $\dot{\boldsymbol{q}}_{dir} = \dot{\boldsymbol{q}}$ and $\dot{\boldsymbol{q}}_{rev} = 0$ if $\dot{\boldsymbol{q}}\boldsymbol{\tau}_{\boldsymbol{act}} > 0$ $\dot{\boldsymbol{q}}_{dir} = 0$ and $\dot{\boldsymbol{q}}_{rev} = \dot{\boldsymbol{q}}$ if $\dot{\boldsymbol{q}}\boldsymbol{\tau}_{\boldsymbol{act}} < 0$	• velocity-proportional term • two terms proportional to hyperbolic tangent of velocity • the direction of the mechanical power is considered
Coulomb + viscous	1773	[33]	$\boldsymbol{\tau}_{f,th} = a_1\,\dot{\boldsymbol{q}} + a_2\text{sign}(\dot{\boldsymbol{q}})$	• velocity-proportional term (viscous term) • constant directional term (Coulomb term)
Dong	2021	[36]	$\boldsymbol{\tau}_{f,th} = a_1\dot{\boldsymbol{q}} + a_2\text{sign}(\dot{\boldsymbol{q}})(1 - e^{-a_3\text{sign}(\dot{\boldsymbol{q}})\dot{\boldsymbol{q}}}) + a_4\text{sign}(\dot{\boldsymbol{q}})e^{-a_5\text{sign}(\dot{\boldsymbol{q}})\dot{\boldsymbol{q}}}$	• velocity-proportional term • constant directional term • two decreasing exponential terms
Gaz (A)	2018	[22]	$\boldsymbol{\tau}_{f,th} = a_1\dot{\boldsymbol{q}} + a_2 + \frac{a_3}{1+e^{-a_4(\dot{\boldsymbol{q}}+a_5)}}$	• velocity-proportional term • constant term • sigmoidal term
Gaz (B)	2019	[23]	$\boldsymbol{\tau}_{f,th} = \frac{a_1}{1+e^{-a_2(\dot{\boldsymbol{q}}+a_3)}} - \frac{a_1}{1+e^{-a_2 a_3}}$	• difference of sigmoidal terms
Grotjahn (A)	2001	[35]	$\boldsymbol{\tau}_{f,th} = a_1\dot{\boldsymbol{q}} + a_2\text{sign}(\dot{\boldsymbol{q}}) + a_3\dot{\boldsymbol{q}}^{1/3}$	• velocity-proportional term • constant directional term • term proportional to the cubic root of velocity
Grotjahn (B)	2001	[35]	$\boldsymbol{\tau}_{f,th} = a_1\dot{\boldsymbol{q}} + a_2\text{sign}(\dot{\boldsymbol{q}}) + a_3\arctan(a_4\dot{\boldsymbol{q}})$	• velocity-proportional term • constant directional term • term proportional to arctangent of velocity
Hao (A)	2021	[38]	$\boldsymbol{\tau}_{f,th} = a_1\text{sign}(\dot{\boldsymbol{q}}) + a_2\dot{\boldsymbol{q}} + a_3\dot{\boldsymbol{q}}^2\text{sign}(\dot{\boldsymbol{q}}) + a_4\dot{\boldsymbol{q}}^3$	• velocity-proportional term • constant directional term • term proportional to square of velocity • term proportional to cube of velocity
Indri (A)	2013	[43]	$\boldsymbol{\tau}_{f,th} = a_1 S_0 + a_2\arctan(a_3\dot{\boldsymbol{q}}) + a_4\dot{\boldsymbol{q}} + (a_5\dot{\boldsymbol{q}}^2)S_0$ with $S_0 = \frac{2}{\pi}\arctan(a_6\dot{\boldsymbol{q}})$	• velocity-proportional term • terms proportional to arctangent of velocity
Makkar	2005	[30]	$\boldsymbol{\tau}_{f,th} = a_1(\tanh(a_2\dot{\boldsymbol{q}}) - \tanh(a_3\dot{\boldsymbol{q}})) + a_4\tanh(a_5\dot{\boldsymbol{q}}) + a_6\dot{\boldsymbol{q}}$	• velocity-proportional term • term proportional to hyperbolic tangent of velocity • difference of hyperbolic terms
Shao	2023	[42]	$\boldsymbol{\tau}_{f,th} = a_1\dot{\boldsymbol{q}} + \frac{2a_2}{\pi}\arctan(a_3\dot{\boldsymbol{q}})$	• velocity-proportional term • term proportional to arctangent of velocity
Wolf	2018	[39]	$\boldsymbol{\tau}_{f,th} = \text{sign}(\dot{\boldsymbol{q}})(a_1 + (a_2 - a_1)e^{-\lvert \frac{\dot{\boldsymbol{q}}}{a_3} \rvert^{a_4}}) + a_5\text{sign}(\dot{\boldsymbol{q}}) \lvert \dot{\boldsymbol{q}} \rvert^{a_6}$	• constant directional term • decreasing exponential term • term proportional to a power of velocity
Zhou	2024	[40]	$\boldsymbol{\tau}_{f,th} = a_1\text{sign}(\dot{\boldsymbol{q}}) \lvert \dot{\boldsymbol{q}} \rvert^{a_2} + a_3\text{sign}(\dot{\boldsymbol{q}})(1 - e^{-\lvert \frac{\dot{\boldsymbol{q}}}{a_4} \rvert^{a_5}}) + a_6\text{sign}(\dot{\boldsymbol{q}})e^{-\lvert \frac{\dot{\boldsymbol{q}}}{a_4} \rvert^{a_5}}$	• term proportional to a power of velocity • constant directional term • two decreasing exponential terms

$\boldsymbol{\tau}_{f,th}$ is the theoretical joint friction torque computed by the friction models, $\dot{\boldsymbol{q}}$ represents the joint velocities, whereas a_k represents each of the friction parameters that have to be optimized to fit the model with the experimental data

and Zhou et al. [40] proposed two friction formulations similar to the ones in [21] and [36], respectively, for the friction behaviour in a humanoid robot and in a 9-DOF custom manipulator, respectively. However, the viscous friction formulations proposed in [39] and [40] are not directly proportional to the velocity, but to a power of it, in order to better capture friction effects at high velocities. To consider the different friction components at low velocities, "dry friction" models have been proposed [41]. The dry friction approach describes friction only at low velocities and therefore it does not cover the entire range of operating velocities of a generic robotic system. For this reason, dry friction models are not considered in this work.

The models presented above often include a *sign* function, which causes a discontinuity at zero velocity that has to be avoided to make the friction models suitable for control

Table 2 Overview on the static friction models (accounting for joint velocity, temperature and/or load torque) considered in this paper

Friction model	Year	Ref.	Formulation	Description
Bittencourt (B)	2012	[21]	$\boldsymbol{\tau_{f,th}} = \text{sign}(\dot{\boldsymbol{q}})(a_1 + a_2 \mid \boldsymbol{\tau_l} \mid + a_3 \mid \boldsymbol{\tau_l} \mid e^{-\mid \frac{\dot{q}}{a_4} \mid^{a_5}} + + (a_6 + a_7\boldsymbol{T})e^{-\mid \frac{\dot{q}}{a_8 + a_9\boldsymbol{T}} \mid^{a_5}}) + + (a_{10} + a_{11}e^{\frac{-\boldsymbol{T}}{a_{12}}})\dot{\boldsymbol{q}}$	• constant term linearly dependent on load • decreasing exponential term linearly dependent on load • decreasing exponential term function of temperature • velocity-proportional term that depends on temperature
Hao (B)	2021	[38]	$\boldsymbol{\tau_{f,th}} = (a_1\text{sign}(\dot{\boldsymbol{q}}) + a_2\dot{\boldsymbol{q}} + a_3\dot{\boldsymbol{q}}^2\text{sign}(\dot{\boldsymbol{q}}) + a_4\dot{\boldsymbol{q}}^3)(1 + a_5(\boldsymbol{T} - T_0))$	• velocity-proportional term • constant directional term • term proportional to square of velocity • term proportional to cube of velocity • linear dependency on temperature
Iskandar	2019	[52]	$\boldsymbol{\tau_{f,th}} = \text{sign}(\dot{\boldsymbol{q}})(F_c + (a_1 - F_c)e^{-\mid \dot{\boldsymbol{q}}/v_s \mid^2}) + F_v\text{sign}(\dot{\boldsymbol{q}}) \mid \dot{\boldsymbol{q}} \mid^{\delta_v}$ with $F_c = a_2 + a_3\boldsymbol{T} + a_4\boldsymbol{T}^2$, $v_s = a_5 + a_6\boldsymbol{T} + a_7\boldsymbol{T}^2$, $F_v = a_8 + a_9\boldsymbol{T} + a_{10}\boldsymbol{T}^2$, $\delta_v = a_{11} + a_{12}\boldsymbol{T} + a_{13}\boldsymbol{T}^2$	• constant directional term • decreasing exponential term • term proportional to a power of velocity • friction coefficients function of temperature
Li	2024	[50]	$\boldsymbol{\tau_{f,th}} = a_1 + \text{sign}(\dot{\boldsymbol{q}})(a_2 + a_3 \mid \dot{\boldsymbol{q}} \mid^{a_4} + + \sqrt{\mid \dot{\boldsymbol{q}} \mid}(a_5 + a_6\boldsymbol{T} + a_7\boldsymbol{T}^{-3}) + a_8{\boldsymbol{\tau_l}}^2)$	• constant offset term • constant directional term • term proportional to a power of velocity • rational polynomial function of temperature • directional term dependent on square load torque
Madsen	2021	[2]	$\boldsymbol{\tau_{f,th}} = \text{sign}(\dot{\boldsymbol{q}})[a_1 e^{-\left(\frac{\mid \dot{q} \mid}{a_2}\right)^{a_3}} + + \sqrt{\mid \dot{\boldsymbol{q}} \mid}(a_4(\boldsymbol{T} - T_0) + a_5(\boldsymbol{T} - T_0)^{-3})] + + a_6\dot{\boldsymbol{q}} + a_7 \mid \dot{\boldsymbol{q}} \mid \dot{\boldsymbol{q}} + a_8\dot{\boldsymbol{q}}^3$	• velocity-proportional term • term proportional to square of velocity • term proportional to cube of velocity • decreasing exponential term • rational polynomial function of temperature
Nevmerzhitskiy	2019	[27]	$\boldsymbol{\tau_{f,th}} = \text{sign}(\dot{\boldsymbol{q}})(a_1 + a_2{\boldsymbol{\tau_l}}^2 + (a_3 + a_4e^{-a_5\boldsymbol{T}}) \mid \dot{\boldsymbol{q}} \mid^{1/2})$	• constant directional term • directional term dependent on square load torque • term proportional to square root of velocity
Simoni	2019	[51]	$\boldsymbol{\tau_{f,th}} = (a_1\text{sign}(\dot{\boldsymbol{q}}) + a_2\dot{\boldsymbol{q}} + a_3\dot{\boldsymbol{q}}^2\text{sign}(\dot{\boldsymbol{q}}) + a_4\dot{\boldsymbol{q}}^3)(a_5 + a_6(\boldsymbol{T} - T_0))$	• velocity-proportional term • constant directional term • term proportional to square of velocity • term proportional to cube of velocity • linear dependency on temperature

$\boldsymbol{\tau_{f,th}}$ is the theoretical joint friction torque computed by the friction models, $\dot{\boldsymbol{q}}$ represents the joint velocities, $\boldsymbol{T}$ indicates the joint temperatures, $\boldsymbol{\tau_l}$ is the load torque, whereas a_k represents each of the friction parameters that have to be optimized to fit the model with the experimental data

purposes [30]. With this aim, Makkar et al. [30] avoided the discontinuity at zero velocity by means of a hyperbolic tangent function (*tanh*). Moreover, the same authors modeled the Stribeck effect as a difference of *tanh* terms [30]. Similarly, Shao et al. [42] represented the Stribeck effect in the joints of a 6-DOF manipulator through an *arctan*, whereas Indri et al. [43] considered the Stribeck and nonlinear effects at high velocities in a 6-DOF Comau SMART NS12 robot thanks to a combination of *arctan* (Indri (A)). Clochiatti et al. [44] modeled friction at low velocities in a UR5e robot with a *tanh* term. In addition, the authors introduced two different parameters for low velocities, depending on the power flow direction to consider that friction behaviour is asymmetric in harmonic drives. In Table 1, $\dot{\boldsymbol{q}}_{dir}$ indicates the velocities when the mechanical power flows out of the motor, whereas $\dot{\boldsymbol{q}}_{rev}$ represents the velocities when the mechanical power flows in the motor.

Differently from the models described above, Gaz et al. [22] modeled friction at low velocities in a 6-DOF UR10 manipulator with a sigmoidal function (Gaz (A)). Similarly, Gaz et al. [23] proposed to model friction in a 7-DOF Franka Emika Panda arm with a difference of sigmoidal functions, without including constant or velocity-proportional terms in the formulation (Gaz (B)). Xiao et al. [45] proposed to consider the joint positions in the friction computation in a 7-DOF KUKA iiwa R820 robot. Nevertheless, in [21] the

authors showed that for a robotic joint, the dependence of friction on the position of the joint position is small and case-specific, as it is mainly related to geometric imperfections.

The values of friction parameters are not unalterable, but can change over time, mainly due to joint temperature and load torque. The change in temperature leads to changes in the properties of the lubricant and contact surfaces. Similarly, the load torque influences the friction behaviour since friction arises from the interaction between contact surfaces and varies according to the applied normal force, which can be modified by the load torque [21].

The load torque mainly influences the Coulomb friction and the Stribeck effect [46]. The authors in [21, 47–49] proposed to model the Coulomb friction as linearly dependent on the absolute value of the load torque. Differently, Nevmerzhitskiy et al. [27] and Li et al. [50] considered a quadratic dependency of Coulomb friction on the load torque. Furthermore, Bittencourt and Gunnarsson [21] and Hassen et al. [49] modeled the Stribeck effect as linearly dependent on the absolute value of the load torque.

Differently from the load torque, the temperature has a significant nonlinear influence on the viscous friction component, and slightly affects the Stribeck effect [46]. To consider the variation in the Stribeck effect, the authors in [21, 27, 49] modeled its dependency on temperature through a decreasing exponential term. Differently, the authors in [38, 51] considered the changes in the Stribeck effect as linear with the temperature, whereas Iskandar and Wolf [52] proposed that the friction coefficients F_c, v_s (see Table 2) of the Stribeck effect change with the temperature as second-degree polynomial functions.

To take into account the influence of the temperature on the viscous friction, different solutions have been developed. For example, Hao et al. [38] and Simoni et al. [51] proposed a model where the viscous friction linearly depends on temperature, whereas Madsen et al. [2] and Li et al. [50] included the dependency of the viscous friction on temperature through a rational polynomial function of the temperature. Differently, the authors in [21, 49] considered the dependency of viscous friction on temperature through a decreasing exponential term. Furthermore, Iskandar and Wolf [52] modeled the friction coefficients that take into account the viscous friction (F_v and δ_v, see Table 2) as second-degree polynomial functions of the temperature.

2.2 Dynamic Friction Models

The dynamic friction models include a state variable that considers the history of the system and are also called "state variable" models [31]. The state variable and the joint velocity are both considered in the computation of the friction torque. Dynamic models are able to better describe friction at rest state and very low velocities with respect to static ones [32]. Therefore, these models are employed especially for the friction model in mechanical systems that have to execute precise movements at low velocities, such as collaborative robotic assembly [53] and fine-positioning linear axes [54]. Table 3 collects the dynamic friction models that are experimentally compared in Section 5.2. These models have been chosen since they have been previously applied to robotic systems in the field of collaborative robotics.

One of the first proposed dynamic friction models is the Dahl model [55], which was developed in 1968 in order to capture the symmetrical hysteresis loops observed in the friction behaviour of ball bearings. The Dahl model was inspired by the stress-strain characteristics of materials, based on the assumption that friction is the result of the interactions of surface asperities, modeled as bristles that can deflect as elastic elements. When the contact surfaces are under stress, friction increases until bonds breaking happens. With reference to the Dahl model formulation reported in Table 3, the state variable z represents the mean bristle deflection. Differently from static models, the Dahl model does not take into account the velocity in the friction computation, but only the relative displacement between the contact surfaces.

Based on this idea, Bliman and Sorine developed a family of dynamic friction models [56–58] for considering stiction, which is the force that has to be overcome to permit the relative motion between the contact surfaces. The same authors underlined that friction does not depend on velocity, but only on the distance covered by one of the two coupled surfaces with respect to the other. However, the Bliman-Sorine model is not able to consider the Stribeck effect, as the Dahl model does [59]. To solve this problem, De Wit et al. [60] proposed in 1995 the LuGre model. Similarly to the Dahl model, the LuGre model is based on the bristle analogy, but considers also the velocity in the friction formulation, introducing a bristle damping term and a function that takes the Stribeck effect into account. Similar to the LuGre model is the elasto-plastic one, developed by Dupont et al. [61]. Its formulation is similar to the LuGre model, but considers the displacement of the surfaces as divided into two different contributions: the elastic and plastic displacements. When the surfaces are sticking, the plastic displacement is constant, whereas during the sliding phase, the elastic displacement remains constant.

Starting from the LuGre model, several modifications have been proposed to improve the friction modelling. Indri et al. [28] observed that the LuGre model shows unfeasible peaks in the friction torque each time the velocity changes its sign rapidly, due to the damping term. To avoid this unrealistic behaviour, the authors proposed to modify the damping term so as to take into account the value of the relative acceleration between the contact surfaces (Indri (B)). This approach has been validated on a Comau Racer3 robot and a Comau Racer7 manipulator. In the same context, Swevers et al. [62] developed the Leuven model, which is also capable of

Table 3 Overview on the dynamic friction models considered in this paper

Friction model	Year	Ref.	Formulation	Description
Dahl	1968	[55]	$\begin{cases} \boldsymbol{\tau_{f,th}} = a_1 z \\ \dot{z} = \dot{\boldsymbol{q}}\,\text{sign}\left(1 - \text{sign}(\dot{\boldsymbol{q}}) a_1 \frac{z}{a_2}\right)\left\lvert 1 - \text{sign}(\dot{\boldsymbol{q}}) a_1 \frac{z}{a_2}\right\rvert^{a_3} \end{cases}$	• linear dependency on the state variable z • not dependent on joint velocity • Stribeck effect not considered
Indri (B)	2020	[28]	$\begin{cases} \boldsymbol{\tau_{f,th}} = a_1 z + f_{\sigma_1}\dot{z} + \tau_{fv} \\ \dot{z} = S_0^2 \dot{\boldsymbol{q}} - a_1 \frac{S_1}{g} z \\ f_{\sigma_1} = \frac{a_2}{\sqrt{a_3\left(\frac{\ddot{q}_{max}}{\dot{q}_{max}}\dot{\boldsymbol{q}}\right)^2 + \ddot{\boldsymbol{q}}^2}} + a_4 \\ g = a_6 + a_7 \frac{2}{\pi}\arctan(S_1 a_8) \\ \tau_{fv} = a_9 \dot{\boldsymbol{q}} + (a_{10}\dot{\boldsymbol{q}}^2) S_0 \end{cases}$ with $S_0 = \frac{2}{\pi}\arctan(a_5 \dot{\boldsymbol{q}})$, $S_1 = S_0 \dot{\boldsymbol{q}}$	• term linearly dependent on the state variable z • dependency on derivative of the state variable $\dot{z}$ function of velocity and acceleration • consider the maximum velocity ($\dot{q}_{max}$) and acceleration ($\ddot{q}_{max}$) during the trajectory • velocity-proportional term • term proportional to the product of the arctangent of velocity and the square of velocity
LuGre	1995	[60]	$\begin{cases} \boldsymbol{\tau_{f,th}} = a_1 z + a_2 \dot{z} + a_3 \dot{\boldsymbol{q}} \\ \dot{z} = \dot{\boldsymbol{q}} - a_1 \frac{\lvert\dot{\boldsymbol{q}}\rvert}{g} z \\ g = a_4 + (a_5 - a_4) e^{-(\dot{\boldsymbol{q}}/a_6)^{a_7}} \end{cases}$	• term linearly dependent on the state variable z • term linearly dependent on derivative of the state variable $\dot{z}$ • velocity-proportional term
Tadese	2022	[26]	$\begin{cases} \boldsymbol{\tau_{f,th}} = a_1 z + a_2 \dot{z} + f_v \\ \dot{z} = \dot{\boldsymbol{q}} - a_1 \frac{\lvert\dot{\boldsymbol{q}}\rvert}{g} z \\ g = a_3 + (a_4 - a_3) e^{-\lvert\dot{\boldsymbol{q}}/a_5\rvert^2} \\ f_v = (a_6 + a_7 \boldsymbol{T})(1 - e^{-\lvert(a_8 + a_9 \boldsymbol{T})\dot{\boldsymbol{q}}\rvert^{(a_{10} + a_{11}\boldsymbol{T})}}) \end{cases}$	• term linearly dependent on the state variable z • term linearly dependent on derivative of the state variable $\dot{z}$ • decreasing exponential term function of temperature

$\boldsymbol{\tau_{f,th}}$ is the theoretical joint friction torque computed by the friction models, $\dot{\boldsymbol{q}}$ represents the joint velocities, $\boldsymbol{T}$ indicates the joint temperatures, $\boldsymbol{\tau_l}$ is the load torque, z represents the state variable, whereas a_k represents each of the friction parameters that have to be optimized to fit the model with the experimental data

capturing pre-sliding hysteresis with nonlocal memory. The generalized Maxwell slip model [63] is a further development of the Leuven model, which models friction as a connection of N single-state friction models. Each single-state friction model is defined by the same dynamic model and has the same input displacement and velocity, but different values of parameters.

However, as for the static models, all the above mentioned dynamic friction models do not consider temperature and load torque changes. Therefore, other authors extended the dynamic friction models in order to take into account these other dependencies. For example, Xiao et al. [53] added a fourth term to the LuGre formulation to account for the effect of the torque load, and applied this model to the joints of a manipulator with 6 DOFs. In the model by Xiao et al., the load-related friction torque is considered dependent on the sign of both the load torque and the velocity. Differently, Tadese et al. [25] proposed an extension of the LuGre model that takes into account the effects of both load torque and temperature in a 6-DOF Indy7 robot. As shown in Table 3, for the temperature term the parameters are function of the temperature and the sign of the velocity. Instead, for the load torque contribution, the parameters depend on the velocity, its sign and the sign of the load torque. Furthermore, the authors in [26] proposed another extension of the LuGre model that considers temperature changes similarly to [25], but not the influence of the load torque.

3 Friction Parameters Identification

In this section, we describe the procedure used for the identification of friction parameters according to each friction model reported in Tables 1, 2, and 3. This general procedure can be applied to any kind of manipulator or robotic system, once the following data are available:

- joint positions $\boldsymbol{q}$;
- joint velocities $\dot{\boldsymbol{q}}$;
- joint accelerations $\ddot{\boldsymbol{q}}$;
- actual joint torques $\boldsymbol{\tau}_{act}$;
- joint temperatures $\boldsymbol{T}$ (only for models that account for temperature changes).

In case the actual joint torques $\boldsymbol{\tau_{act}}$ are not directly available from the robot controller, these can be computed from the actual motor currents $\boldsymbol{I_m}$, knowing the vector of the gear ratios $\boldsymbol{i_r}$, and the vector of the motor torque constants $\boldsymbol{k_t}$, as:

$$\boldsymbol{\tau}_{act} = \boldsymbol{i_r}\, \boldsymbol{k_t}\, \boldsymbol{I_m} \tag{1}$$

To extrapolate the friction contribution $\boldsymbol{\tau}_f$ from the joint torques $\boldsymbol{\tau}_{act}$, the whole dynamics of the robot needs to be considered. The torque contribution $\boldsymbol{\tau}_{dyn}$ not related to friction during the trajectory ($\boldsymbol{q}$, $\dot{\boldsymbol{q}}$, $\ddot{\boldsymbol{q}}$) can be derived from the dynamic model of the manipulator as:

$$\boldsymbol{\tau}_{dyn} = \boldsymbol{M}(\boldsymbol{q})\ddot{\boldsymbol{q}} + \boldsymbol{C}(\boldsymbol{q}, \dot{\boldsymbol{q}})\dot{\boldsymbol{q}} + \boldsymbol{g}(\boldsymbol{q}) \tag{2}$$

where $\boldsymbol{M}(\boldsymbol{q})$ represents the mass matrix of the robot, which accounts for the inertia of links, motors and reducers. $\boldsymbol{C}(\boldsymbol{q}, \dot{\boldsymbol{q}})\dot{\boldsymbol{q}}$ considers the Coriolis and centrifugal effects, whereas $\boldsymbol{g}(\boldsymbol{q})$ represents gravity. Assuming that masses, centers of mass, and inertia parameters of the robot are well known, as well as the robot parameters, $\boldsymbol{\tau}_{dyn}$ can be computed from joint positions, velocities, and accelerations. However, in cases where the available robot dynamics is uncertain or inaccurate, an alternative approach based on interval arithmetic, as in [64], can be considered.

Therefore, the joint friction torques $\boldsymbol{\tau}_f$ can be computed as:

$$\boldsymbol{\tau}_f = \boldsymbol{\tau}_{act} - \boldsymbol{\tau}_{dyn} \tag{3}$$

In the following, the joint friction torques extrapolated from the experimental data are indicated with $\boldsymbol{\tau}_{f,exp}$ to distinguish them from the theoretical ones ($\boldsymbol{\tau}_{f,th}$) obtained with each of the friction models.

The parameters a_k of the considered friction models (Tables 1, 2, and 3) can be derived exploiting the values of $\boldsymbol{\tau}_{f,exp}$, fitting each model with the experimental data from the robot under consideration. For this purpose, the root-mean-square (RMS) error $e_j^{\tau_f,RMS}$ of the difference between the experimental and the theoretical joint friction torques is minimized for each joint of the robot as:

$$e_j^{\tau_f,RMS}(\boldsymbol{x}) = \sqrt{\frac{1}{n}\sum_{i=1}^{n}(\tau_{f,exp,ij} - \tau_{f,th,ij}(\boldsymbol{x}))^2},\ j = 1, ..., N \tag{4}$$

where n is the number of samples of the considered trajectory of the robot, N represents the number of robot joints, whereas $\boldsymbol{x}$ is the vector of the parameters a_k of the considered friction model. The minimization of $e_j^{\tau_f,RMS}$ is casted as a bounded optimization problem formulated as follows:

$$\begin{aligned} &\min_{\boldsymbol{x}\in\boldsymbol{\chi}} e_j^{\tau_f,RMS}(\boldsymbol{x}) \\ &\boldsymbol{\chi} = \left[\boldsymbol{x}^L\ \boldsymbol{x}^U\right]^T \end{aligned} \tag{5}$$

where $\boldsymbol{x}$ is the vector of the optimization variables (the friction model parameters a_k), whereas $\boldsymbol{\chi}$ includes the lower ($\boldsymbol{x}^L$) and upper ($\boldsymbol{x}^U$) bounds of the optimization variables. The number of elements of $\boldsymbol{x}$ depends on the number of parameters of the friction model to be optimized. For instance, in the Coulomb model [33] the optimization variables are a_1 and a_2 ($k = 2$), whereas in the LuGre model [60] $\boldsymbol{x}$ includes a_1, a_2, a_3, a_4, a_5, a_6, and a_7 ($k = 7$).

The modelling accuracy of the different friction models is first evaluated in terms of joint friction torque errors as:

$$\boldsymbol{e}^{\boldsymbol{\tau}_f} = \boldsymbol{\tau}_{f,exp} - \boldsymbol{\tau}_{f,th} \tag{6}$$

This quantitative index measures the capability of each friction model to represent the joint torques of the robot, and provides a first indication of the performance of each friction model in the prediction of the dynamic behavior of the robotic system.

Furthermore, the total electrical energy consumed by the robot during the trajectory is also considered to estimate the capability of each friction model in reproducing the energetic behaviour of the robot (when used in the complete dynamic formulation of the manipulator). In this context, to simplify the computation of the consumed energy, we represent the AC brushless motors, normally mounted in a robotic joint, as equivalent DC motors thanks to the Park-Clark transformation [65]. In this way, the theoretical electrical power $W_{e,th,j}$ for the j-th motor can be calculated through the following equation [44], which accounts for both the Joule losses and the mechanical losses in the electrical motors of the manipulator:

$$W_{e,th,j} = \frac{1}{k_{m,j}^2}\left(\frac{\tau_{dyn,j} + \tau_{f,th,j}}{i_{r,j}}\right)^2 + \frac{k_{b,j}}{k_{t,j}}\dot{q}_j(\tau_{dyn,j} + \tau_{f,th,j}),\quad j = 1, ..., N \tag{7}$$

where $k_{m,j}$ is the motor constant of the j-th joint, $k_{b,j}$ represents the back-emf constant of the j-th joint, and $k_{t,j}$ indicates the torque constant of the j-th joint. Furthermore, $\tau_{dyn,j}$ is j-th joint theoretical dynamic torque, $\tau_{f,th,j}$ represents the j-th joint theoretical friction torque, $i_{r,j}$ indicates the j-th joint gear ratio, whereas $\dot{q}_j$ is the j-th joint velocity. The sum $\tau_{dyn,j} + \tau_{f,th,j}$ represents the theoretical actual joint torques, needed to perform the desired trajectory.

The j-th motor experimental electrical power $W_{e,exp,j}$ can be computed from Eq. 7, substituting $\tau_{dyn,j} + \tau_{f,th,j}$ with the experimental actual joint torques $\tau_{act,j}$, leading to the

following equation:

$$W_{e,exp,j} = \frac{1}{k_{m,j}^2}\left(\frac{\tau_{act,j}}{i_{r,j}}\right)^2 + \frac{k_{b,j}}{k_{t,j}}\dot{q}_j\tau_{act,j}, \quad j = 1, ..., N \tag{8}$$

Then, the theoretical and experimental total electrical energies consumed by the robot ($E_{e,tot,th}$ and $E_{e,tot,exp}$, respectively) can be computed as the sum over the robot joints of the integral of the theoretical and experimental electrical power, respectively, over time, as follows:

$$E_{e,tot,th} = \sum_{j=1}^{N}\int_0^T W_{e,th,j}\,dt \tag{9}$$

$$E_{e,tot,exp} = \sum_{j=1}^{N}\int_0^T W_{e,exp,j}\,dt \tag{10}$$

Finally, the error difference between the electrical energy computed with each friction model and the one obtained from the experimental data can be evaluated:

$$e_{tot}^{E_{e,tot}} = E_{e,tot,exp} - E_{e,tot,th} \tag{11}$$

This second quantitative index based on the energy consumption of the robot serves as a further measure of the effectiveness of each friction model, when used together with the dynamic model of the robot, offering insights into the practical applicability of each friction model. By analyzing both joint torque representation and energy consumption error, we can comprehensively evaluate the overall accuracy and efficiency of the friction models under various operating conditions.

4 Experimental Setup

The friction parameters identification procedure described in Section 3 is applied to a UR5e manipulator available at the Mechatronics and Robotics Lab of University of Udine (Italy), shown in Fig. 2. The UR5e robot has 6 DOFs, a payload of 5 Kg, and an operational reach of 850 mm. This manipulator mounts HFUS-25-2SH strain wave gearing in the first three joints, and HFUS-14-2SH strain wave gearing in the last three joints, both produced by Harmonic Drive SE [44]. Both types of reducers have a gear ratio equal to 100:1; the first type presents a maximum input speed of 7500 rpm and a repeated peak torque of 157 Nm, whereas the second exhibits a maximum input speed of 14000 rpm and a repeated peak torque of 28 Nm [66]. The dynamic and electro-mechanic parameters of the robot used to computed

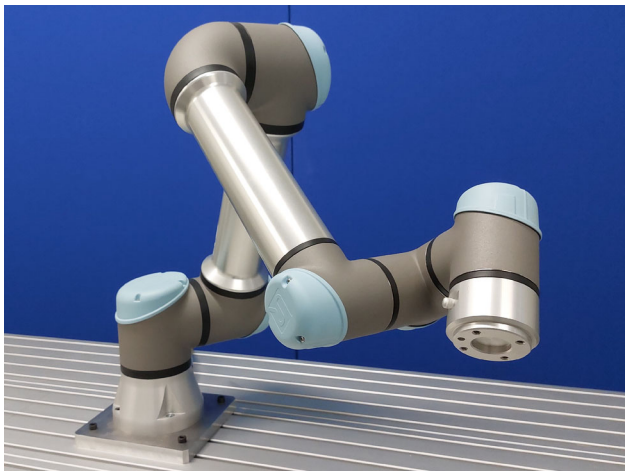

Fig. 2 The UR5e robot used in the experimental tests

τ_{dyn} and the theoretical energetic expenditure $E_{e,tot,th}$ are taken from [44].

The robot is controlled with a computer running Ubuntu 18.04 with an Intel Core i5-10600K CPU @4.10 GHz and 31.2 GB of RAM. ROS (Robot Operating System) Melodic and Python 3.6 are used to program the robot, which is controlled via TCP/IP connection. The Real Time Data Exchange (RTDE) protocol is adopted for real-time communication and data acquisition at 500 Hz. From the control interface, the required data listed in Section 3 can be acquired. However, the actual joint torques are not directly available from the controller of the UR5e robot, and have to be obtained from the actual motor currents through Eq. 1.

For the experimental tests, bespoke excitation trajectories are designed to cover the whole range of joint velocities and accelerations of the robot. For the static friction models only accounting for joint velocity, the trajectory for the robot is planned in the joint space using trapezoidal speed profiles (Test (1)). To explore the whole range of velocities of the robot, six random points are chosen in the joint space so as to bring at least one joint close to its velocity limit for each of the five point-to-point motions, while meeting the robot kinematics and dynamics joint limits. In this way, we ensure that the robot is working in challenging conditions with multiple changes of direction in its workspace, and the inertial load is highly variable during the test. The 3D path of the robot end-effector corresponding to the trajectory of Test (1) is shown in Fig. 3a.

Regarding the static friction models that also account for temperature changes, the tests for the robot are defined so as to repeat the same trajectory multiple times and catch the warming up of the mechanical system. In this case, we adopt a fifth-degree polynomial motion law planned in the joint space between each couple of a set of twenty way points (Test (2)). The way points are selected randomly with the

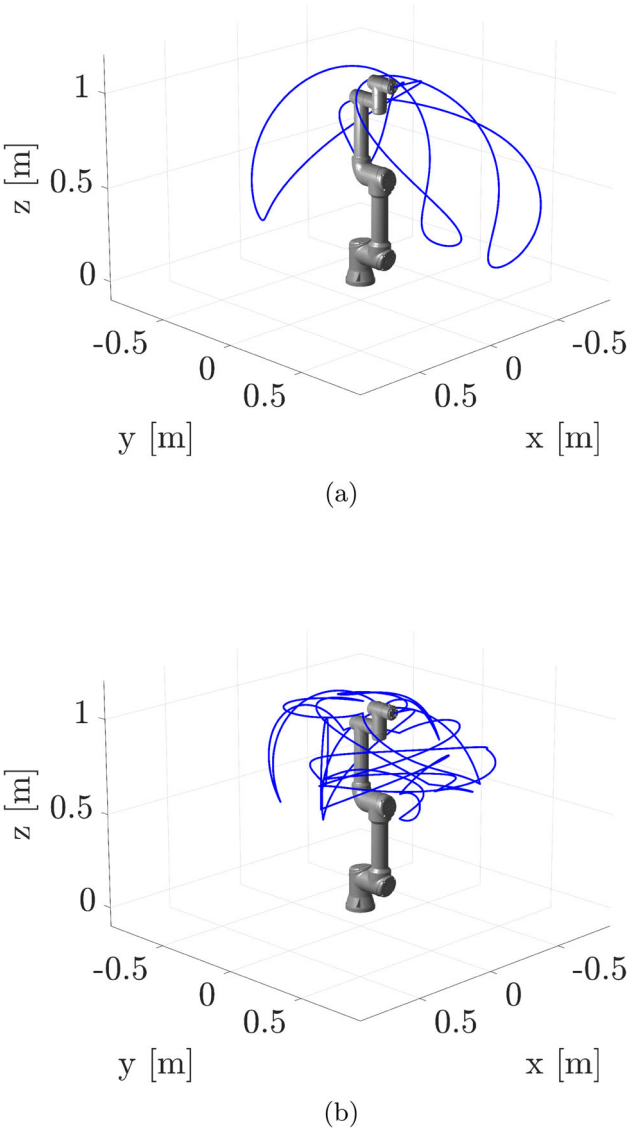

Fig. 3 Representation of the 3D path of the robot end-effector in the Cartesian space planned for Test (1) (**a**), and for Test (2) (**b**). The configuration of the robot shown in the figures represents its initial and final joint positions in the experimental tests

same approach of Test (1). Fifth-degree polynomial trajectories are chosen to ensure a smooth robot motion and avoid sudden robot stops due to abrupt accelerations at low temperatures of the robot joints (the high viscosity of the lubricant can cause a joint deviation from the reference value [67]). The entire trajectory lasts sixty seconds and it is repeated ninety times. The 3D path of the robot during one of the repeated trajectories of Test (2) is shown in Fig. 3b.

The trajectory of Test (1) is however not suitable for friction parameters identification of the dynamic friction models that do not consider temperature changes, since it is too short to cause any temperature variation. Therefore, for the dynamic friction models the data acquired during the first trajectory of Test (2) are used (sixty seconds, a duration considered sufficient for evaluating the influence of the history of the system). For the dynamic friction models that also take into account the temperature changes, the data acquired from all the ninety repeated trajectories of Test (2) are considered.

The considered friction models reported in Tables 1, 2, and 3 are implemented in Matlab 2020b, using a computer equipped with 32 GB of RAM and an Intel Core i5-10600K CPU @4.10 GHz processor running Windows 10 Pro. In the friction models that also account for load effects, the load torque τ_l is computed as τ_{dyn}. Regarding the dynamic friction models, the state variable z is obtained from its derivative $\dot{z}$ through integration with the forward Euler method. For each friction model and for each robot joint, the optimization problem of Eq. 5 is solved with the constrained nonlinear multivariable Matlab function *fmincon* implementing the sequential quadratic programming (SQP) method. In order to better explore the design domain χ for each of the considered models, we perform a multi-start optimization, randomly selecting 20 points within each parameter bound. Finally, for each friction model, among the 20 optimal combinations of parameters found, only the one with the smallest $e_j^{\tau_f,RMS}$ is considered.

5 Experimental Results

In this section we present the experimental results obtained by fitting the considered static and dynamic friction models to the experimental data obtained with the UR5e robot. In Section 5.1 the performance of the static friction models in reproducing the joint friction torques of the robot and computing its total energy consumption are presented, whereas the results of the dynamic friction models are illustrated in Section 5.2.

5.1 Comparison of Static Friction Models

Figures 4, 5, 6, and 7 and Table 4 report the experimental results for the static friction models accounting for joint velocity only, listed in Table 1. Figure 4 depicts the trajectory of Test (1) in terms of joint positions $\boldsymbol{q}$, velocities $\dot{\boldsymbol{q}}$, accelerations $\ddot{\boldsymbol{q}}$, and end-effector velocities $\dot{\boldsymbol{x}}$, $\dot{\boldsymbol{y}}$, $\dot{\boldsymbol{z}}$ over time. From the graph of the end-effector velocities, it can be seen that the end-effector exceeds sometimes its maximum velocity, equal to 1 m/s. This points out that the excitation trajectory of Test (1) is challenging for the robot and is therefore suitable to stress the system over a wide velocity range. Figure 5 shows the joint torques $\boldsymbol{\tau_{act}}$ and experimental friction torques $\boldsymbol{\tau_{f,exp}}$ over time during Test (1). Figure 6 reports a comparison between the experimental joint friction torque for the first two joints of the robot and the theoretical one computed

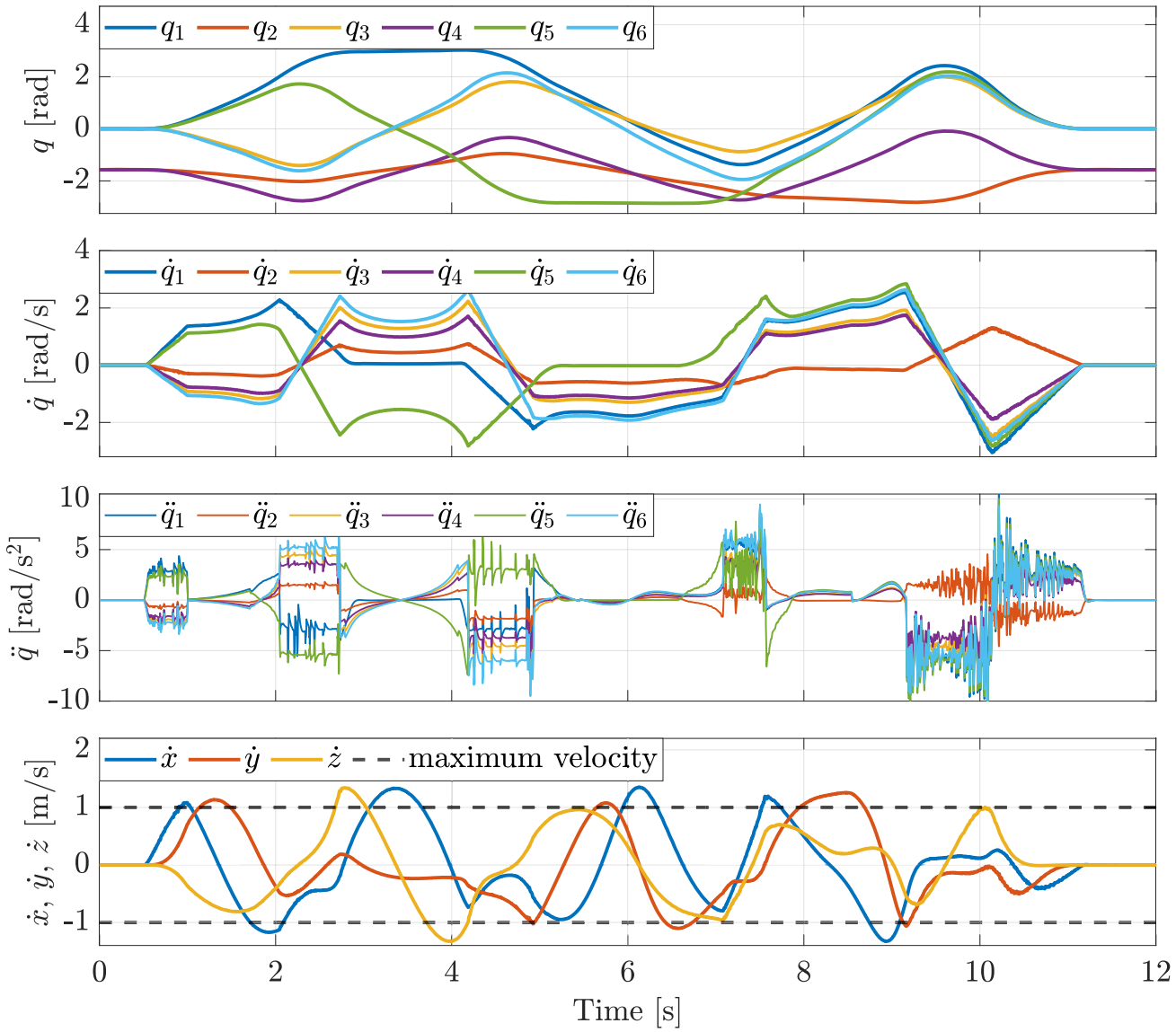

Fig. 4 Joint positions $\boldsymbol{q}$, velocities $\dot{\boldsymbol{q}}$, accelerations $\ddot{\boldsymbol{q}}$, and end-effector velocities $\dot{\boldsymbol{x}}$, $\dot{\boldsymbol{y}}$, $\dot{\boldsymbol{z}}$ over time during Test (1)

by means of three different models, i.e., the ones in [22, 33], and [43]. From Fig. 6 it can be seen that the three different models approximate the experimental data differently, since they include different functions in their formulation. This evidence proves that each considered friction model is suitable for a different situation, depending on the friction behaviour and working conditions.

Furthermore, Fig. 7 illustrates the box plots of the joint friction torque errors (computed from Eq. 6) of the considered models for the first two joints. In the box plots, the middle mark represents the median, while the bottom and top of each box indicate the first and third quartiles. Whiskers refer to the most extreme data points that are not considered outliers. We report both the box plots obtained considering the whole range of joint velocities and those retrieved by taking into account only the joint velocities comprised between ± 0.1 rad/s, in order to asses the ability of the models to describe friction torques also at low velocities. A precise dynamic modelling at low velocities is fundamental in collaborative robotics, where the robots are often limited in speed for safety of the human operator [64].

Finally, Table 4 reports, for the considered static models, the joints friction errors for the first and second joints as mean $\pm$ standard deviation, the theoretical electrical energy consumed by the robot during the trajectory (derived from Eq. 7), the electrical energy error between the theoretical and the experimental data (obtained with Eq. 11), and the corresponding percentage error. The experimental results illustrated in Fig. 7 and in Table 4 allow us to compare the considered static friction models and assess their capabilities

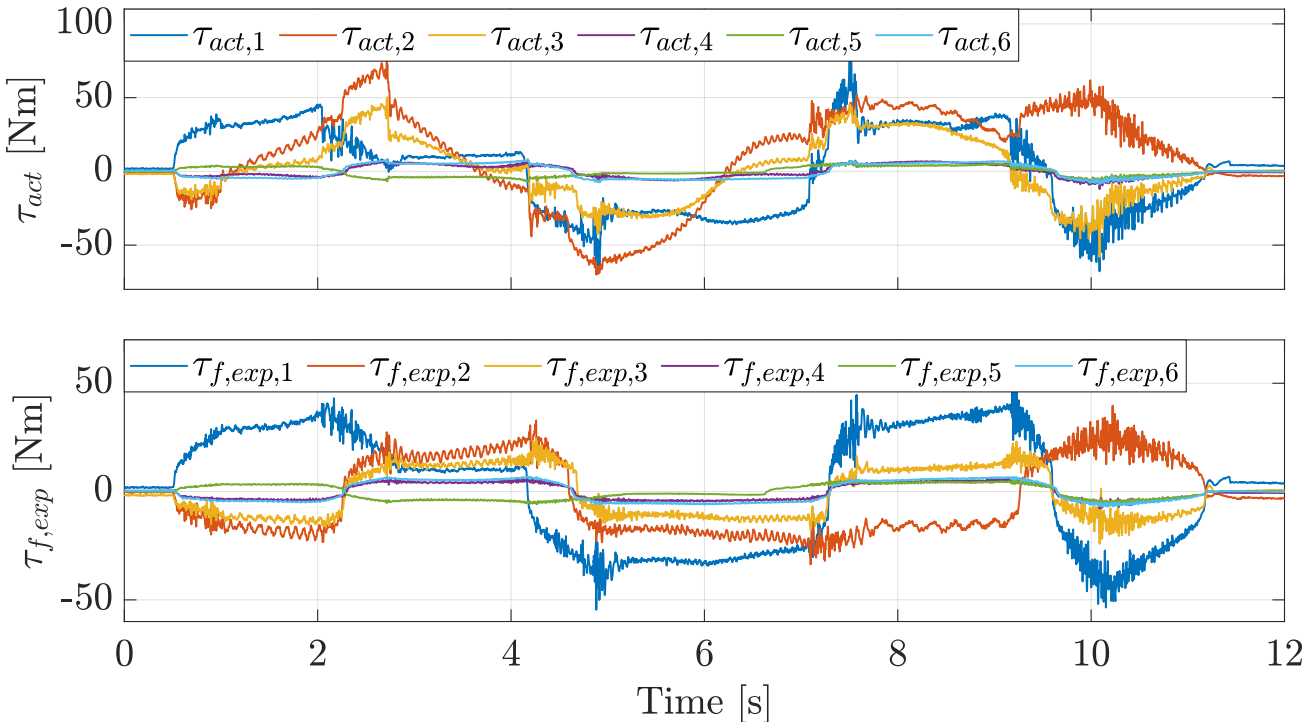

Fig. 5 Joint torques $\boldsymbol{\tau_{act}}$ and experimental friction torques $\boldsymbol{\tau_{f,exp}}$ over time during Test (1)

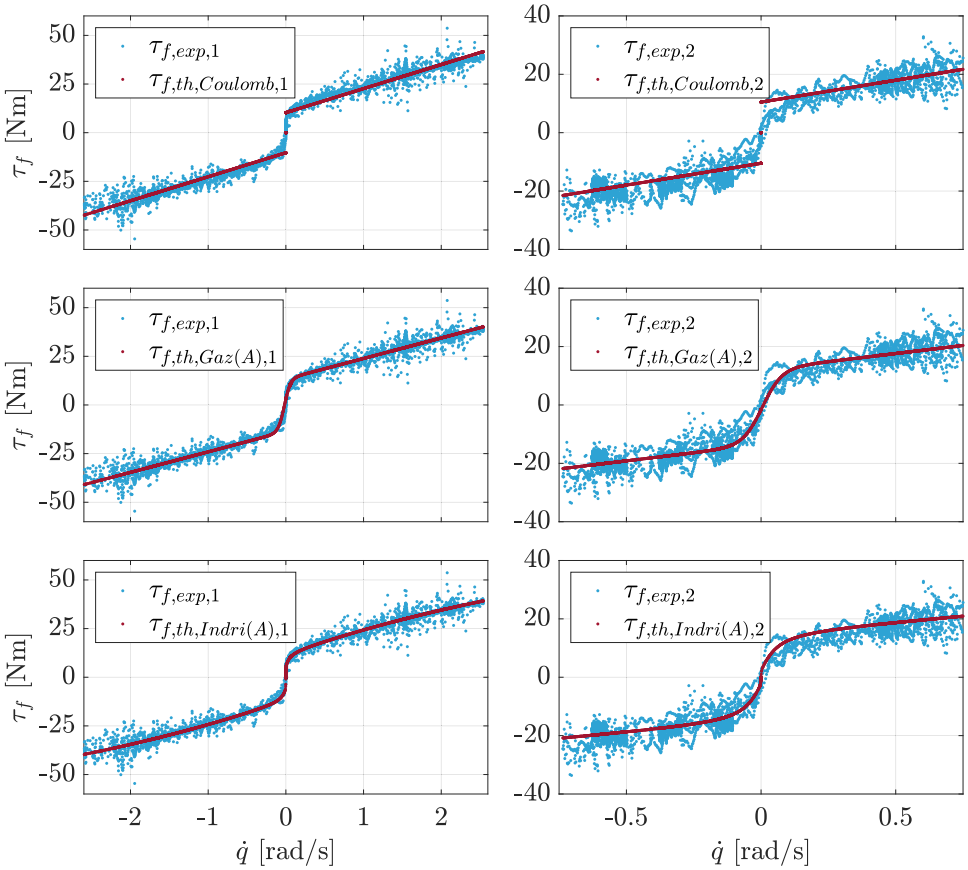

Fig. 6 Friction torques over joint velocities for joints 1 and 2, considering three different models for approximating the experimental data: Coulomb [33], Gaz (A) [22], and Indri (A) [43]

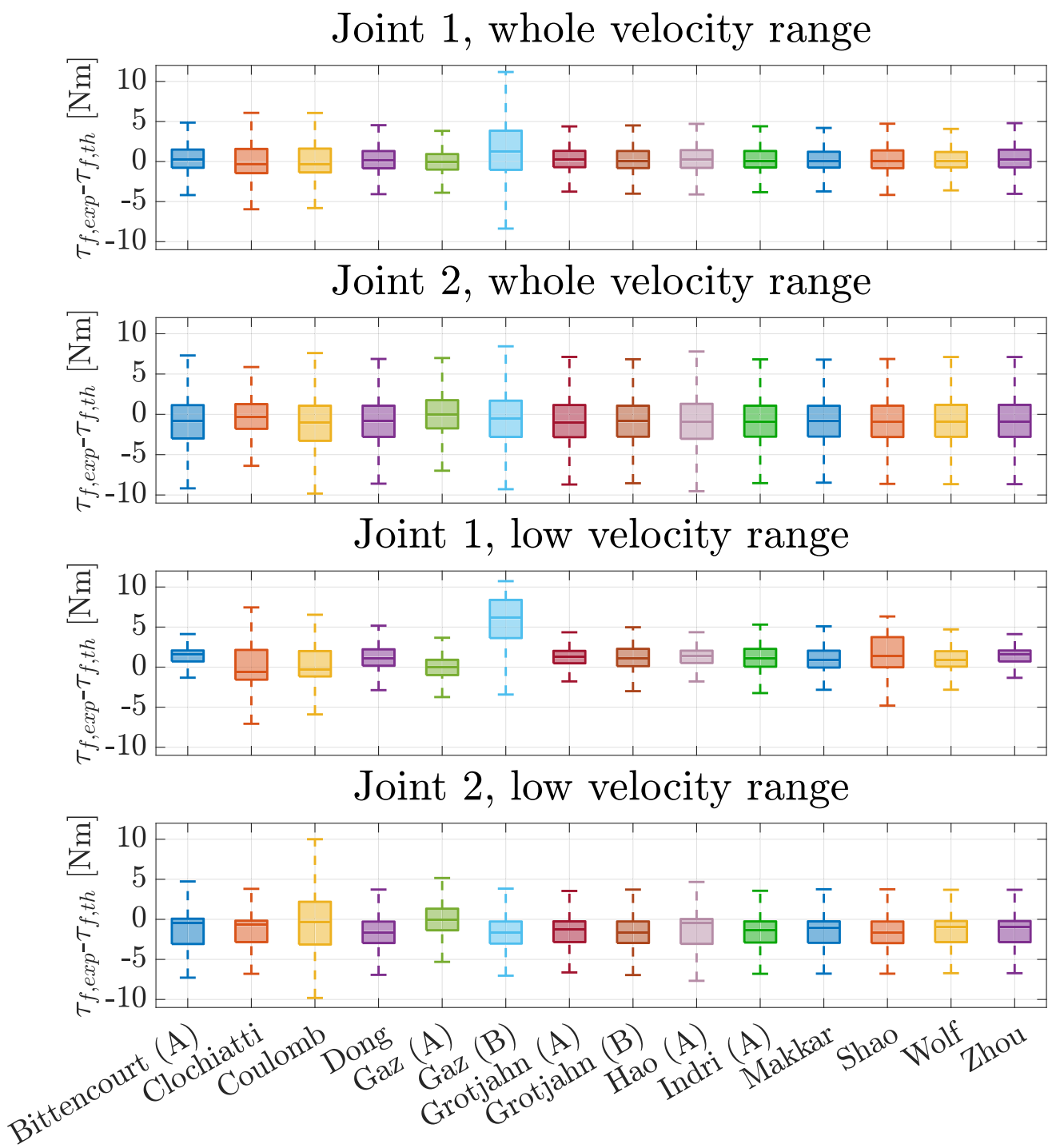

Fig. 7 Box plot representation of the torque errors for the different models for joints 1 and 2 for the whole range of velocities for Test (1); box plot representation of the torque errors for the different models for joints 1 and 2 for velocities between -0.1 and 0.1 rad/s for Test (1)

to correctly predict the joint friction torques of the robot and in reproducing the energetic behaviour of the robot. More in detail, the model Gaz (A) [22] is the one that shows lower values of friction torque errors for both joints 1 and 2, whereas the lowest errors in the computation of the total electrical energy are obtained when using the model proposed by Clochiatti et al. [44].

Figures 8, 9, 10, 11, and 12 and Table 5 show the experimental results for the static friction models that account for joint velocity, temperature and/or load torque, reported in

Table 4 Experimental results for the static friction models accounting for joint velocity only: friction torque errors (mean ± standard deviation) for joints 1 ($e_1^{\tau_f}$) and 2 ($e_2^{\tau_f}$), total electrical energy spent during the trajectory ($E_{e,tot,th}$) computed with the different models, total electrical energy errors obtained with the models with respect to the experimental data ($e_{tot}^{E_{e,tot}}$), and corresponding percentage error ($e_{tot}^{E_{e,tot},\%}$) with respect to the $E_{e,tot,exp} = 772.57\ J$

Friction model	Ref.	$e_1^{\tau_f}$ [Nm]	$e_2^{\tau_f}$ [Nm]	$E_{e,tot,th}$ [J]	$e_{tot}^{E_{e,tot}}$ [J]	$e_{tot}^{E_{e,tot},\%}$ [%]
Bittencourt (A)	[21]	0.32 ± 2.66	-0.86 ± 3.08	775.13	−2.56	−0.33
Clochiatti	[44]	0.02 ± 2.86	-0.26 ± 2.63	772.98	−0.41	−0.05
Coulomb	[33]	0.05 ± 3.07	-1.12 ± 3.70	775.37	−2.80	−0.36
Dong	[36]	0.29 ± 2.59	-0.78 ± 2.96	775.07	−2.50	−0.32
Gaz (A)	[22]	0.00 ± 2.44	0.00 ± 2.94	774.85	−2.28	−0.30
Gaz (B)	[23]	1.34 ± 4.34	-0.36 ± 3.44	767.21	5.36	0.69
Grotjahn (A)	[35]	0.30 ± 2.55	-0.78 ± 3.00	775.17	−2.60	−0.34
Grotjahn (B)	[35]	0.29 ± 2.57	-0.79 ± 2.96	775.08	−2.51	−0.32
Hao (A)	[38]	0.29 ± 2.73	-0.89 ± 3.24	775.23	−2.65	−0.34
Indri (A)	[43]	0.25 ± 2.53	-0.78 ± 2.95	775.10	−2.53	−0.33
Makkar	[30]	0.23 ± 2.52	-0.76 ± 2.95	775.05	−2.48	−0.32
Shao	[42]	0.31 ± 2.61	-0.79 ± 2.96	775.07	−2.50	−0.32
Wolf	[39]	0.23 ± 2.51	-0.77 ± 2.99	775.14	−2.57	−0.33
Zhou	[40]	0.32 ± 2.62	-0.77 ± 2.99	774.86	−2.29	−0.30

Table 2. Figure 8 illustrates the joint positions $\dot{\boldsymbol{q}}$, velocities $\dot{\boldsymbol{q}}$, accelerations $\ddot{\boldsymbol{q}}$, and end-effector velocities $\dot{x}$, $\dot{y}$, $\dot{z}$ over time during a cycle of Test (2). Figure 9 depicts the joint torques $\boldsymbol{\tau_{act}}$ and the experimental friction torques $\boldsymbol{\tau_{f,exp}}$ over time during the first and the ninetieth cycles, showing that from the first to the ninetieth cycle (i.e., after one hour and a half of continuous working of the robot) both $\boldsymbol{\tau_{act}}$ and $\boldsymbol{\tau_{f,exp}}$ are reduced due to the increasing of temperature. The effect of the temperature variation can be noted also from Figs. 10 and 11, which compare the experimental joint friction torques for the first two joints with the ones obtained with the models by [50] and [52], respectively. Figures 10 and 11 show that the friction torque decreases with the increasing of temperature. Comparing these two figures, we can observe slightly differences in the friction approximation of the two considered models, highlighting again that different friction formulations do not model friction in the same way.

Moreover, Fig. 12 illustrates the box plots of the joint friction torque errors of the considered models for the first two joints. Similarly to Fig. 7, Fig. 12 depicts the difference between the experimental friction torque and the theoretical ones for the entire range of joint velocities and considering only the joint velocities comprises between ±0.1 rad/s. Finally, Table 5 reports the difference between the experimental friction torque and the considered theoretical ones, the electrical energy consumed by the robot during the trajectory computed with the friction models, the error in the computation of the electrical energy consumed between the theoretical and the experimental data, and the corresponding percentage error. With the experimental results showed in Fig. 12 and in Table 5, we can compare the considered models and evaluate their ability of capture the influence of temperature and load torque on the friction behaviour in the joints of the UR5e robot. In this case, the model by Li et al. [50] shows the best performance in representing the friction torques and in the computation of the consumed energy with respect to alternative approaches.

5.2 Comparison of Dynamic Friction Models

To evaluate the modelling performance of the dynamic friction models, we exploit the data acquired from Test (2). The trajectory of one cycle of the robot is reported in Fig. 8, whereas Fig. 9 shows the joint torques and joint friction torques over time during Test (2). As explained in Section 4, for the dynamic friction models that do not account for temperature changes (i.e., Dahl [55], Indri (B) [28], LuGre [60]) only the first cycle of Test (2) is considered, whereas for the model by Tadese et al. [26] that also takes into account the temperature changes, all cycles of Test (2) are adopted.

Figures 13 and 14 represent a comparison between the experimental joint friction torques and the theoretical ones obtained with the models by [60] and [28], respectively, for all the six joints of the UR5e robot. Observing the whole velocity range, it can be seen that, for a single velocity, friction can assume different values. This is due to the fact that the dynamic friction models take into account not only the current state, but also the history of the system, leading to different friction values for a same state of the system. Moreover, in Figs. 13 and 14 a magnified view of friction behavior at very low velocities (between ±0.02 rad/s) is provided. This particular highlights the presence of the hysteresis phenomenon, which is typical characteristic of harmonic drives [68]. This behaviour cannot be considered by static friction models due to their formulation, and it is particularly relevant when a robotic system operates at low velocities.

Furthermore, Fig. 15 reports the box plots of the joint friction torque errors for the first and second joint between

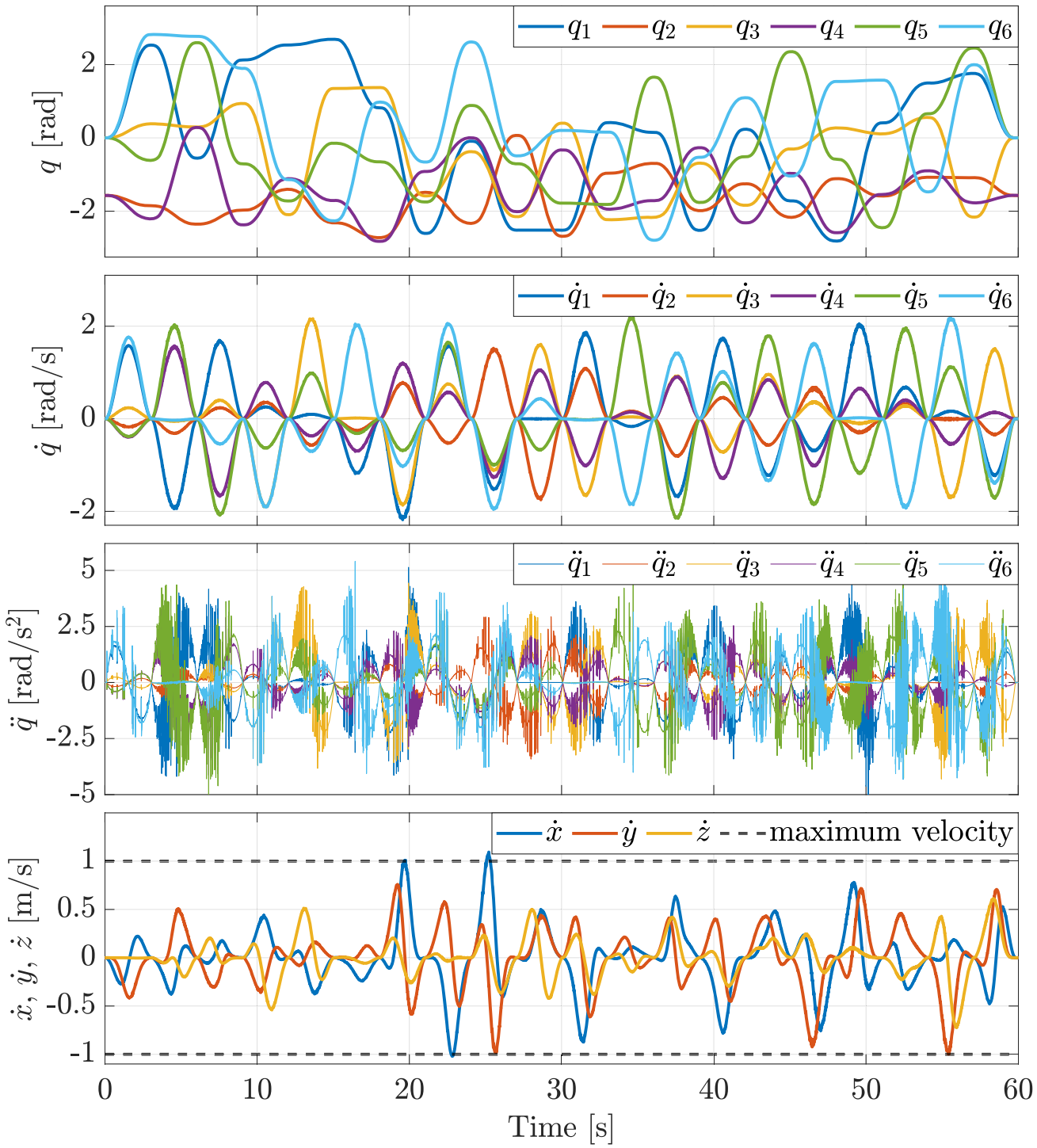

Fig. 8 Joint positions $\boldsymbol{q}$, velocities $\dot{\boldsymbol{q}}$, accelerations $\ddot{\boldsymbol{q}}$, and end-effector velocities $\dot{x}$, $\dot{y}$, $\dot{z}$ over time during one cycle of Test (2)

the experimental data and each considered model. Also in this case, both the box plots obtained considering the whole range of joint velocities and taking into account only the joint velocities comprised between ±0.1 rad/s are depicted. From Fig. 15 it can be seen that the Dahl model [55] presents an error larger than the other models, since it does not consider the influence of the value of velocity in the friction behaviour.

Finally, Table 6 illustrates the experimental results of the considered dynamic friction models in terms of joint friction torque error for the first two joints, theoretical electrical

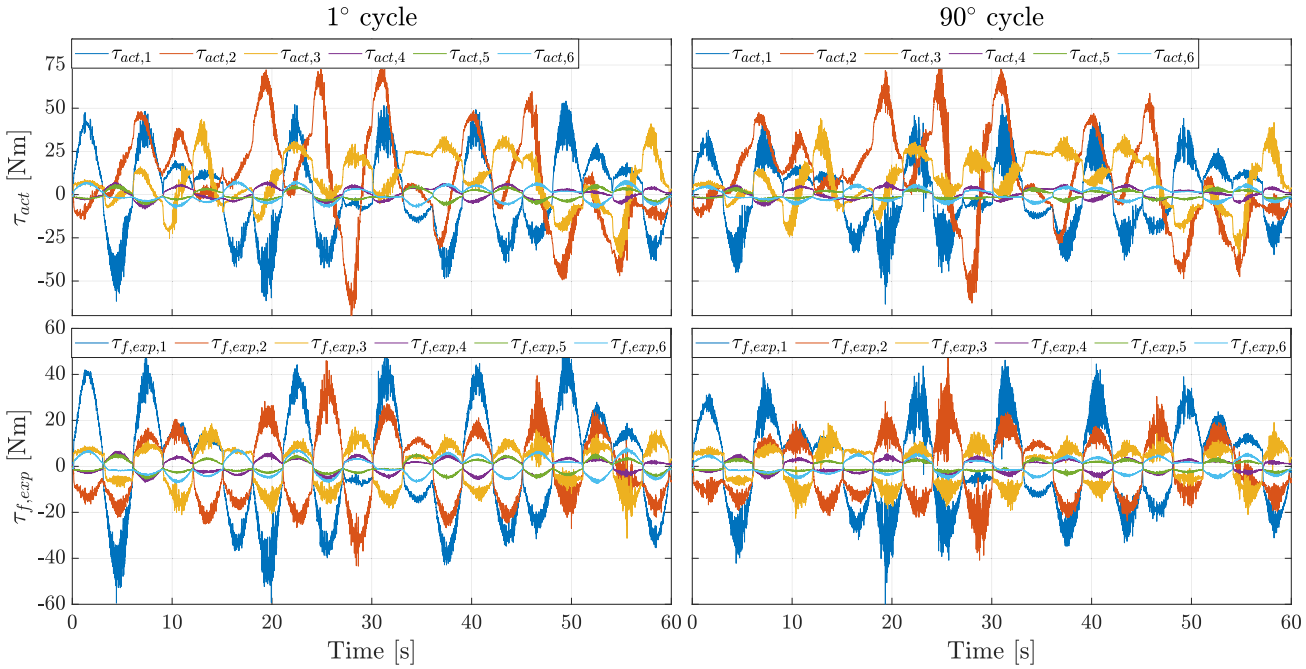

Fig. 9 Joint torques $\boldsymbol{\tau_{act}}$ and experimental friction torques $\boldsymbol{\tau_{f,exp}}$ over time during the first (left) and the ninetieth cycle (right) of Test (2)

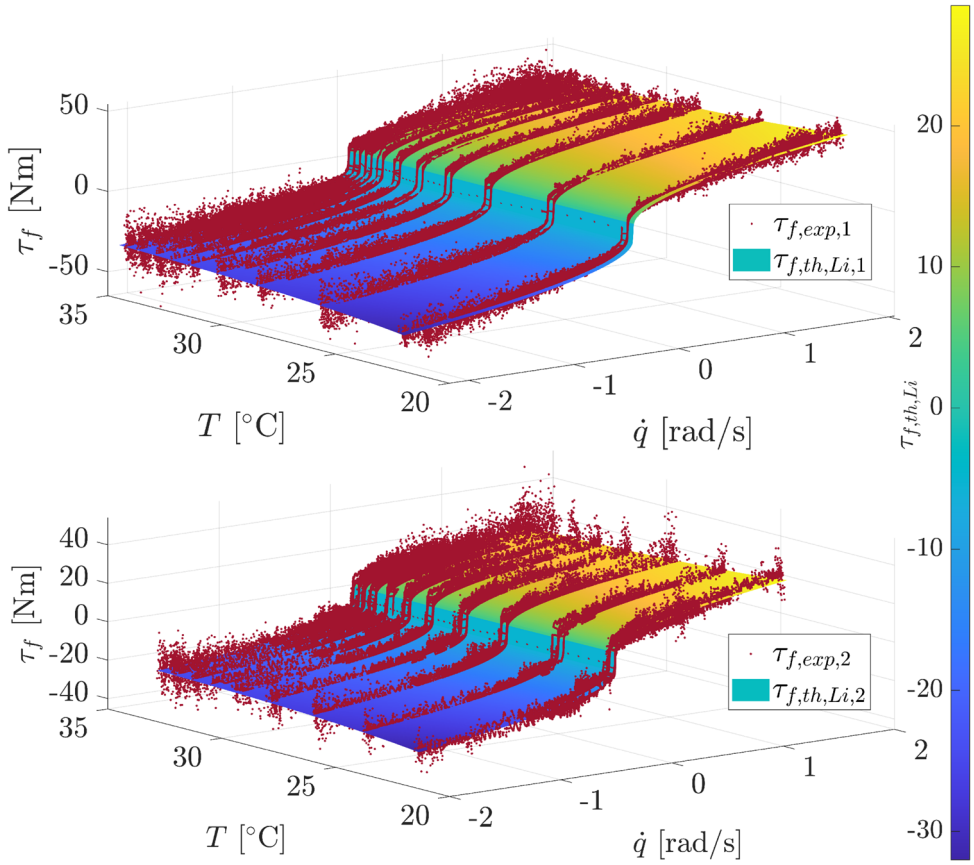

Fig. 10 Friction torques over joint velocities and joint temperatures for joints 1 and 2 for Test (2), considering the data obtained with the model in [50]

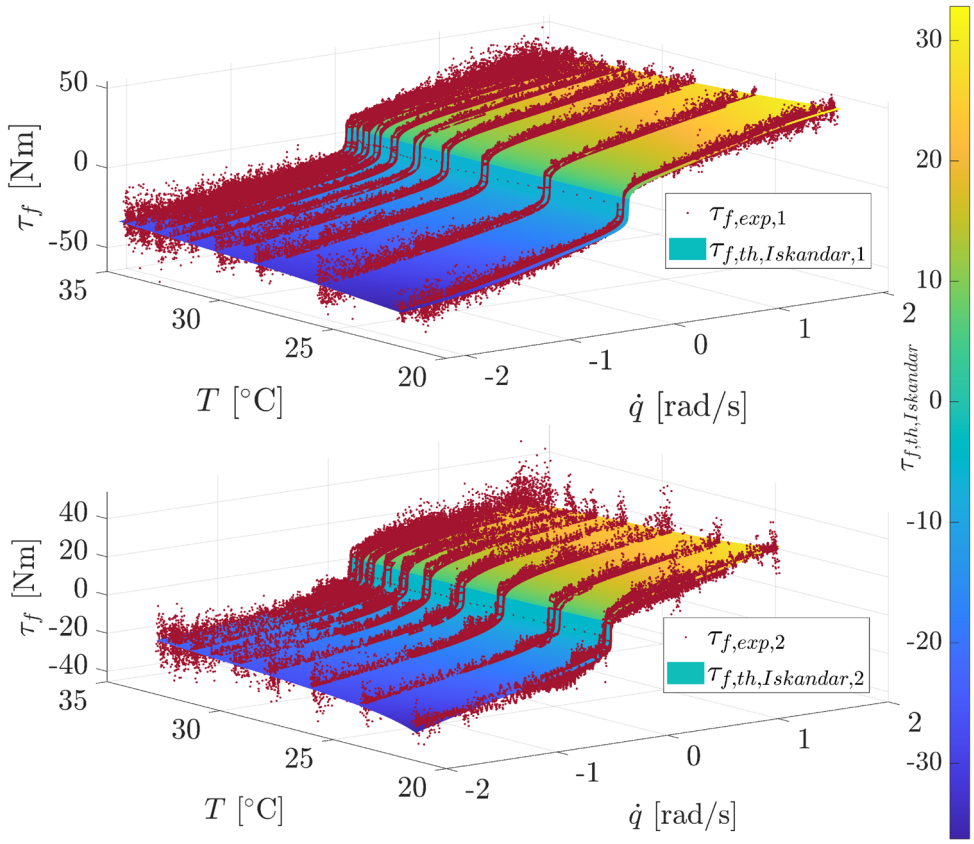

Fig. 11 Friction torques over joint velocities and joint temperatures for joints 1 and 2 for Test (2), considering the data obtained with the model in [52]

energy expenditure $E_{e,tot,th}$ during the trajectory, electrical energy error between the experimental data and the results obtained with each model, and the corresponding percentage error. For the Tadese model [26], experimental electrical energy consumed $E_{e,tot,exp}$ is equal to 17452 J, whereas for the other three dynamic friction models considered it is equal to 2121 J. Also from Table 6 a larger error of the Dahl model with respect to the other considered models can be observed. Moreover, from Fig. 15 and Table 6 we are able to evaluate the friction modelling capabilities of the considered dynamic friction models, both for the entire range of velocities and for low velocities.

6 Discussion

A wide number of friction models exists in the present literature: each model includes different contributions and describes friction behaviour in alternative ways (see Fig. 6), resulting suitable for different scenarios, systems, and working conditions. Static friction models have the advantage of a simpler structure and generally few parameters, making them computationally efficient [32]. However, most static friction models do not take into account changes in temperature and load torque, nor the history of the system, limiting their application when the working conditions vary significantly over time.

For example, the Coulomb model [33] exhibits one of the simplest structures, since it includes only two parameters. Nevertheless, its friction modelling error with respect to the other static models is indeed rather small if we consider the whole range of velocities (excluding the model in [23], which is evidently the less accurate one), as can be seen from Fig. 7 and Table 4. This small difference is due to the friction approximation of the model at low velocities. Focusing on the energy consumption, a friction modelling error at low velocities is scarsely relevant, since in this case the electrical power is generally low, leading to a limited electrical energy error, as can be seen from Table 4. Alternative static friction models proposed different formulations to consider the friction behaviour at low velocities. Nevertheless, despite their complexity and how they consider the various components of friction, their accuracy is relatively comparable (see Fig. 7 and Table 4).

Among the static friction models, some of them incorporate the effects of temperature and load torque, making them more versatile as they can represent the system behaviour under variable operational conditions. These models are particularly useful in applications where temperature and load torque change significantly influences friction effects, such as in high-speed machinery or systems exposed to changing

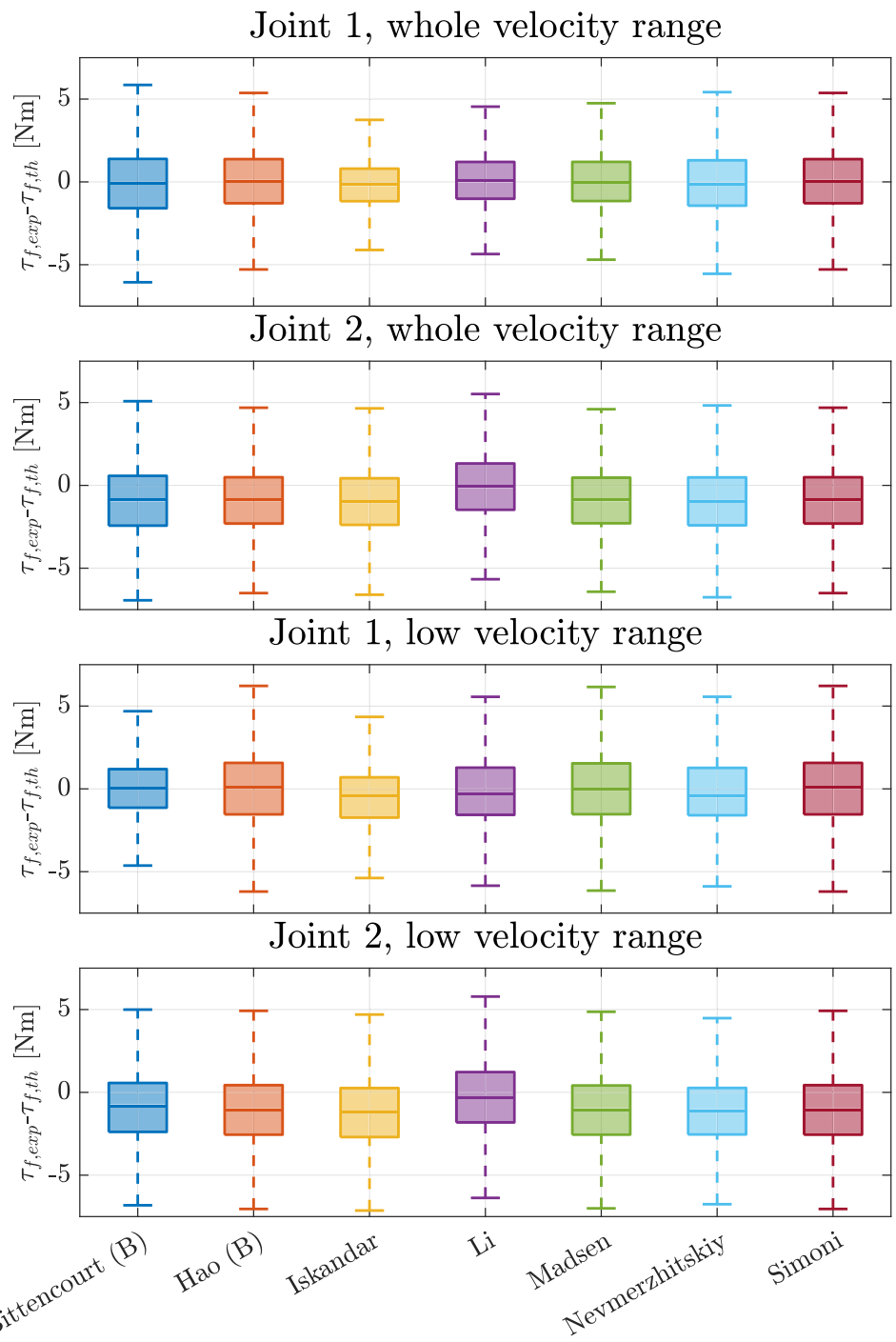

Fig. 12 Box plot representation of the torque errors for the different models for joints 1 and 2 for the whole range of velocities for Test (2); box plot representation of the torque errors for the different models for joints 1 and 2 for velocities comprises between -0.1 and 0.1 rad/s for Test (2)

environmental conditions. Generally, these models are extensions of the ones accounting for joint velocity only in order to capture the influence of temperature and load torque on friction behaviour. Among the considered models, their accuracy in terms of friction modelling is comparable, as it can be observed from Fig. 12 and Table 5. Considering instead their ability in representing the energetic behaviour of the robotic system, from Table 5 it can be noted that the model that provides the best results is the one in [50].

Differently from the static friction models, the dynamic ones are more sophisticated, capable of capturing complex phenomena like low-speed hysteresis and the dependency of friction on past system states. Figures 13 and 14 highlight the ability of dynamic friction models in describing the low-speed hysteresis phenomenon. However, these models include a differential formulation for describing the system behavior more accurately, leading to higher computational times and the availability of the system history, which can

Table 5 Experimental results for the considered static friction models accounting for joint velocity, temperature and load torque: friction torque errors (mean ± standard deviation) for joints 1 ($e_1^{\tau_f}$) and 2 ($e_2^{\tau_f}$), total electrical energy spent during the trajectory ($E_{e,tot,th}$) computed with the different models, total electrical energy errors obtained with the models with respect to the experimental data ($e_{tot}^{E_{e,tot}}$), and corresponding percentage error ($e_{tot}^{E_{e,tot},\%}$) with respect to the $E_{e,tot,exp} = 17452\ J$

Friction model	Ref.	$e_1^{\tau_f}$ [Nm]	$e_2^{\tau_f}$ [Nm]	$E_{e,tot,th}$ [J]	$e_{tot}^{E_{e,tot}}$ [J]	$e_{tot}^{E_{e,tot},\%}$ [%]
Bittencourt (B)	[21]	-0.20 ± 3.19	-0.85 ± 3.07	17512	−60.78	−0.35
Hao (B)	[38]	-0.06 ± 2.82	-0.85 ± 2.71	17525	−73.36	−0.42
Iskandar	[52]	-0.27 ± 2.36	-0.91 ± 2.51	17513	−61.50	−0.35
Li	[50]	0.00 ± 2.46	0.00 ± 2.50	17457	−5.09	−0.03
Madsen	[2]	-0.10 ± 2.71	-0.86 ± 2.67	17514	−61.97	−0.36
Nevmerzhitskiy	[27]	-0.16 ± 2.97	-0.92 ± 2.71	17519	−67.86	−0.39
Simoni	[51]	-0.06 ± 2.81	-0.85 ± 2.71	17525	−73.36	−0.42

be challenging to obtain and implement in real-time applications. Figure 15 and Table 6 show that the Dahl model [55] is by far the less accurate in modelling friction in the whole range of velocities of a robotic system, since it does not consider the velocity value in the friction torque computation. For the other three dynamic friction models considered (i.e., Indri (B) [28], LuGre [60], and Tadese [26]), Fig. 15 and Table 6 show that their accuracy is similar, both in terms of friction modelling and electrical energy computation.

From the analysis of the considered friction models provided above, it appears that static friction models are simpler and computationally more efficient, but they lack to consider friction at low velocities adequately. For this reason, they are more suitable where the robotic or mechatronic system operates at significant joint velocities and there are limited transitions at velocities close to zero, and these transitions happen with high accelerations [32]. Furthermore, static friction models accounting also for joint temperature and load torque can be useful when the working conditions change over time. Conversely, dynamic friction models are more complex and require higher computational times, but they

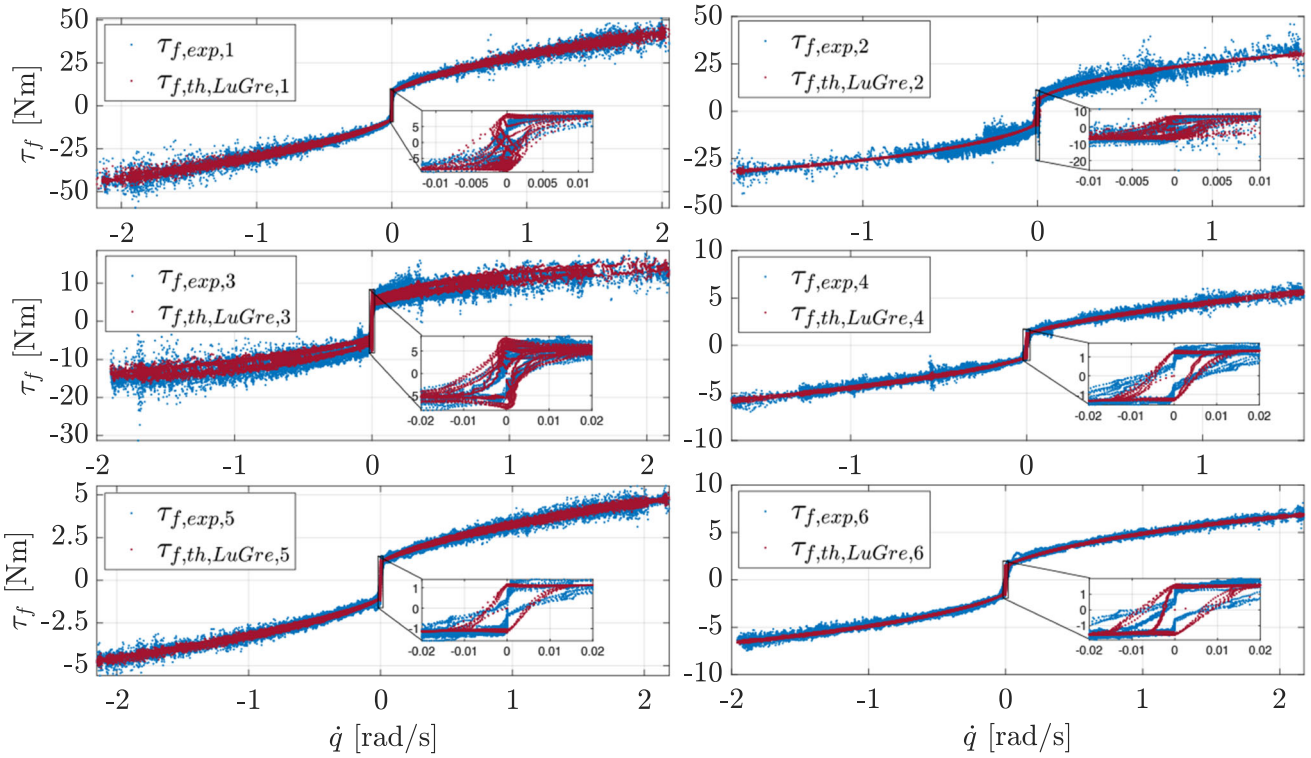

Fig. 13 Friction torques over joint velocities for all the six joints for the first cycle of Test (2), considering the data obtained with the LuGre model [60]

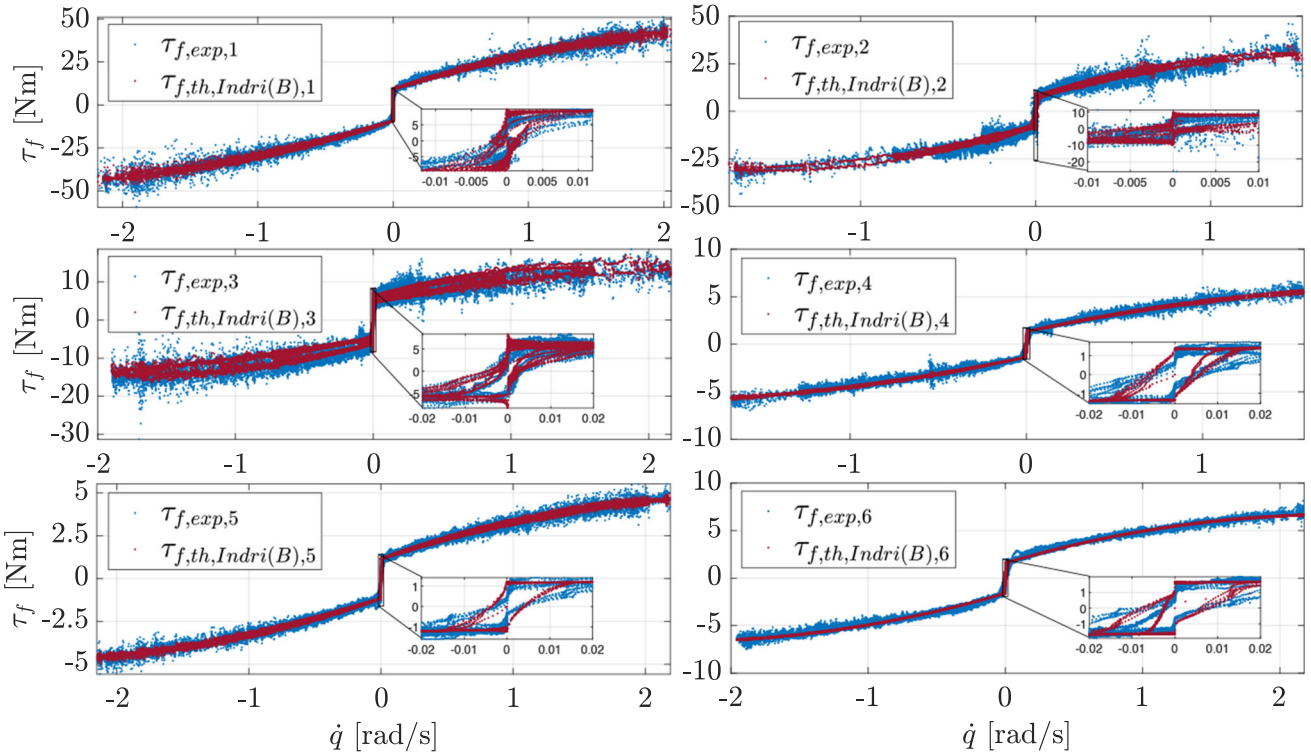

Fig. 14 Friction torques over joint velocities for all the six joints for the first cycle of Test (2), considering the data obtained with model in [28]

are able to better represent friction at low velocities, as for example in collaborative robotic applications [53, 64].

In this work, we have compared various friction models, delineating their advantages and disadvantages to provide a comprehensive guideline for selecting and applying the most suitable. This comparison is particularly useful in the field of collaborative robotics, where robots often are operated among a wide range of operative speeds, and friction forces represent a major source of energy losses. By understanding the strengths and limitations of each model, practitioners can make informed decisions that enhance the performance, efficiency, and reliability of robotic systems.

7 Conclusions

In this paper, the state of the art and an experimental comparison of friction models for robotic manipulators have been presented. We investigated both static and dynamic friction models, analyzing their formulation, features, and capabilities. For some of the models considered here, not only speed dependance but also load torque and temperature have been taken into account. Then, an extensive experimental comparison of twenty-five friction models on a UR5e robot with 6 DOFs is provided. The experimental results evidenced the capabilities of the considered models to capture different friction components. Static friction models generally exhibit a simpler formulation, but they do not consider friction at low velocities properly. Furthermore, only few static models are able to take into account the effects of temperature and load torque on friction behaviour. Dynamic models instead can better represent friction in the entire range of velocities, especially at very low velocities at a cost of increased complexity. However, almost all the considered models are able to provide satisfactory results, both in terms of friction torque prediction and energy consumption evaluation.

The comparison of the selected models evidence that, since they consider various friction contributions and in different ways, the different friction models are suitable for different applications and working conditions. Consequently, this paper can be used as a guideline in the selection of the friction model best suited to the considered operating condition. Furthermore, these models can be considered for friction modelling in various fields of robotics, such as design of control algorithms, trajectory planning for energy efficiency purposes, and applications for collaborative robotics.

Future work will include the investigation and development of friction models based on artificial intelligence (AI) approaches to accurately predict friction behavior under different conditions. This will involve exploring various machine learning algorithms for friction modelling [69, 70], friction compensation [71, 72], or adaptation of existing

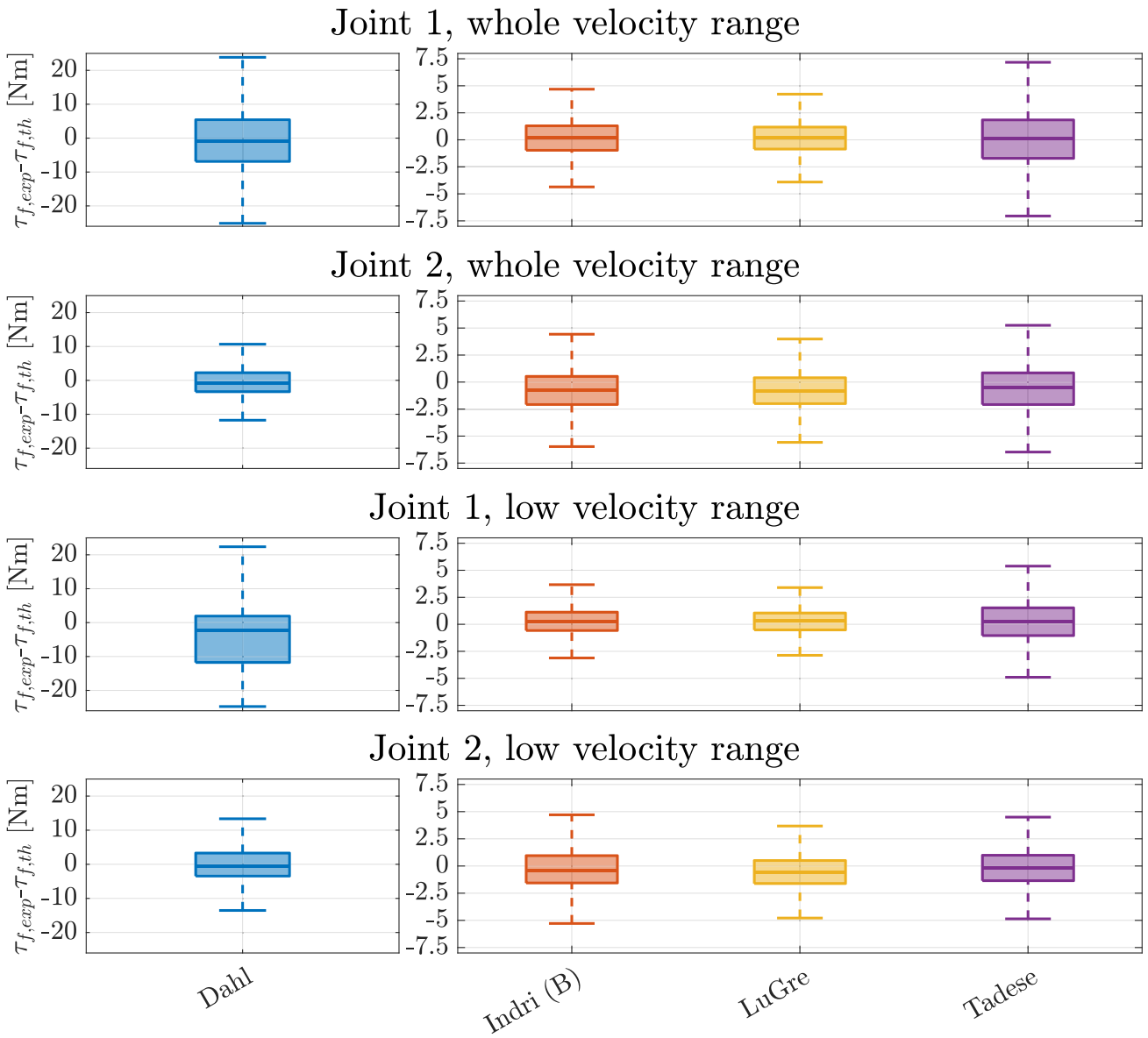

Fig. 15 Box plot representation of the torque errors for the different models for joints 1 and 2 for the whole range of velocities for the considered dynamic models; box plot representation of the torque errors for the different models for joints 1 and 2 for velocities comprises between -0.1 and 0.1 rad/s for the considered dynamic models

Table 6 Experimental results for the considered dynamic friction models: friction torque errors (mean ± standard deviation) for joints 1 ($e_1^{\tau_f}$) and 2 ($e_2^{\tau_f}$), total electrical energy spent during the trajectory ($E_{e,tot,th}$) computed with the different models, total electrical energy errors obtained with the models with respect to the experimental data ($e_{tot}^{E_{e,tot}}$), and corresponding percentage error ($e_{tot}^{E_{e,tot},\%}$) with respect to the $E_{e,tot,exp}$

Friction model	Ref.	$e_1^{\tau_f}$ [Nm]	$e_2^{\tau_f}$ [Nm]	$E_{e,tot,th}$ [J]	$e_{tot}^{E_{e,tot}}$ [J]	$e_{tot}^{E_{e,tot},\%}$ [%]
Dahl	[55]	-0.70 ± 9.14	-0.36 ± 5.19	1680	441.23	20.80
Indri (B)	[28]	0.12 ± 1.94	-0.73 ± 2.34	2126	−4.56	−0.22
LuGre	[60]	0.12 ± 1.89	-0.74 ± 2.26	2128	−6.59	−0.31
Tadese	[26]	0.04 ± 3.27	-0.64 ± 2.86	17337	114.92	0.66

friction models [73]. Additionally, we aim to integrate these AI-based models with existing simulation frameworks to enhance their predictive capabilities and efficiency. Finally, extensive validation and testing will be carried out to ensure the robustness and reliability of the proposed AI-based models in practical applications.

A Optimal Friction Parameters

Table 7 reports the optimal friction parameters obtained by fitting each of the selected twenty-five models to the experimental data of the UR5e robot. The values reported in the table are related to the friction modelling of joint 1 of the robot.

Table 7 Optimal friction parameters of the considered friction models for the first joint of the robot

Friction model	Ref.	Optimal friction parameters a_k
Static friction models (accounting for joint velocity only)		
Bittencourt (A)	[21]	$a_1 = -1388$; $a_2 = 1395$; $a_3 = -12.62$; $a_4 = 1.12$; $a_5 = 96.30$
Clochiatti	[44]	$a_1 = 12.03$; $a_2 = 10.84$; $a_3 = 10.79$
Coulomb	[33]	$a_1 = 12.35$; $a_2 = 10.30$
Dong	[36]	$a_1 = 10.45$; $a_2 = 13.61$; $a_3 = 16.34$; $a_4 = 3.24$; $a_5 = 16.34$
Gaz (A)	[22]	$a_1 = 10.54$; $a_2 = -13.55$; $a_3 = 26.89$; $a_4 = 25.37$; $a_5 = 0.02$
Gaz (B)	[23]	$a_1 = 71.87$; $a_2 = 1.79$; $a_3 = 0.01$
Grotjahn (A)	[35]	$a_1 = 5.58$; $a_2 = 3.14$; $a_3 = 15.92$
Grotjahn (B)	[35]	$a_1 = 10.13$; $a_2 = 3.01$; $a_3 = 7.24$; $a_4 = 22.65$
Hao (A)	[38]	$a_1 = 8.06$; $a_2 = 22.66$; $a_3 = -7.26$; $a_4 = 1.24$
Indri (A)	[43]	$a_1 = 6.03$; $a_2 = 4.06$; $a_3 = 899.76$; $a_4 = 13.04$; $a_5 = -0.98$; $a_6 = 15.59$
Makkar	[30]	$a_1 = 7.07$; $a_2 = 0.84$; $a_3 = -17.93$; $a_4 = 4.04$; $a_5 = 88486$; $a_6 = 8.37$
Shao	[42]	$a_1 = 10.25$; $a_2 = 14.12$; $a_3 = 33.75$
Wolf	[39]	$a_1 = 306.24$; $a_2 = -4.30$; $a_3 = 44.35$; $a_4 = 0.89$; $a_5 = 18.29$; $a_6 = 0.10$
Zhou	[40]	$a_1 = 19.33$; $a_2 = 0.58$; $a_3 = -379.32$; $a_4 = 264.32$; $a_5 = 366.69$; $a_6 = 5.50$
Static friction models (accounting for joint velocity, temperature and/or load torque)		
Bittencourt (B)	[21]	$a_1 = -5.26$; $a_2 = -0.04$; $a_3 = 0.43$; $a_4 = -3.72$; $a_5 = 1887$; $a_6 = 15.83$; $a_7 = -0.07$; $a_8 = -38.75$; $a_9 = 77.72$; $a_{10} = 10.93$; $a_{11} = 169.30$; $a_{12} = 6.95$;
Hao (B)	[38]	$a_1 = 8.16$; $a_2 = 40.32$; $a_3 = -25.34$; $a_4 = 6.92$; $a_5 = -0.02$
Iskandar	[52]	$a_1 = 0.05$; $a_2 = 0.63$; $a_3 = 1.77$; $a_4 = -0.04$; $a_5 = 8.11$; $a_6 = -0.70$; $a_7 = 0.01$; $a_8 = 21.16$; $a_9 = 0.19$; $a_{10} = -0.01$; $a_{11} = 0.18$; $a_{12} = 0.01$; $a_{13} = -0.0001$
Li	[50]	$a_1 = -0.18$; $a_2 = -0.82$; $a_3 = 6.99$; $a_4 = 0.06$; $a_5 = 16.77$; $a_6 = -0.06$; $a_7 = 0.001$; $a_8 = -0.008$
Madsen	[2]	$a_1 = 6.36$; $a_2 = 0.44$; $a_3 = 2.99$; $a_4 = -0.28$; $a_5 = 40.68$; $a_6 = 50.39$; $a_7 = -30.75$; $a_8 = 7.57$
Nevmerzhitskiy	[27]	$a_1 = 4.26$; $a_2 = -0.01$; $a_3 = 20.40$; $a_4 = -87.40$; $a_5 = 309.89$
Simoni	[51]	$a_1 = 10.09$; $a_2 = 49.89$; $a_3 = -31.35$; $a_4 = 8.57$; $a_5 = 0.81$; $a_6 = -0.01$
Dynamic friction models		
Dahl	[55]	$a_1 = 26350$; $a_2 = 81.09$; $a_3 = 25.43$
Indri (B)	[28]	$a_1 = 90124$; $a_2 = 1699$; $a_3 = 29859$; $a_4 = 496.74$; $a_5 = 6198$; $a_6 = 9.25$; $a_7 = 3646$; $a_8 = 0.04$; $a_9 = -71.88$; $a_{10} = -4.13$
LuGre	[60]	$a_1 = 102467$; $a_2 = 562.39$; $a_3 = -91.75$; $a_4 = 74716$; $a_5 = 7.70$; $a_6 = 1002$; $a_7 = 0.94$
Tadese	[26]	$a_1 = 14753$; $a_2 = 467.25$; $a_3 = 31.20$; $a_4 = 10.31$; $a_5 = -0.89$; $a_6 = 10.26$; $a_7 = -0.11$; $a_8 = 74.88$; $a_9 = 4870$; $a_{10} = 717.03$; $a_{11} = -32.26$

Author Contributions LS and PB contributed to the study conception and design. Material preparation, data collection, and analysis were performed by GF and LS. The first draft of the manuscript was written by GF and LS, and all authors commented on previous versions of the manuscript. All authors read and approved the final manuscript.

Funding Open access funding provided by Università degli Studi di Udine within the CRUI-CARE Agreement. This research has been developed within the Laboratory for BigData, IoT, Cyber Security (LABIC) funded by Friuli Venezia Giulia region, and the Laboratory for Artificial Intelligence for Human-Robot Collaboration (AI4HRC) funded by Fondazione Friuli. This study was carried out within the Interconnected Nord-Est Innovation Ecosystem (iNEST) and received funding from the European Union Next-GenerationEU (National Recovery and Resilience Plan, Mission 4.2, Investment 1.5, D.D. 1058 23/06/2022, ECS 00000043). This manuscript reflects only the authors' views and opinions, neither the European Union nor the European Commission can be considered responsible for them.

Availability of Data and Materials Not applicable.

Declarations

Competing Interests Not applicable.

Code Availability Not applicable.

Ethics Approval Not applicable.

Consent to Participate Not applicable.

Consent for Publication Not applicable.

References

1. Xiao, B., Yin, S.: Exponential tracking control of robotic manipulators with uncertain dynamics and kinematics. IEEE Trans. Industr. Inf. **15**(2), 689–698 (2018)
2. Madsen, E., Rosenlund, O.S., Brandt, D., Zhang, X.: Adaptive feedforward control of a collaborative industrial robot manipulator using a novel extension of the Generalized Maxwell-Slip friction model. Mech. Mach. Theory **155**, 104109 (2021)
3. Huynh, H.N., Assadi, H., Rivière-Lorphèvre, E., Verlinden, O., Ahmadi, K.: Modelling the dynamics of industrial robots for milling operations. Robot. Comput.-Integr. Manuf. **61**, 101852 (2020)
4. Han, Y., Wu, J., Liu, C., Xiong, Z.: An iterative approach for accurate dynamic model identification of industrial robots. IEEE Trans. Rob. **36**(5), 1577–1594 (2020)
5. Li, W., Han, Y., Wu, J., Xiong, Z.: Collision detection of robots based on a force/torque sensor at the bedplate. IEEE/ASME Trans. Mechatron. **25**(5), 2565–2573 (2020)
6. Morinaga, S., Kosuge, K.: Compliant motion control of manipulator's redundant DOF based on model-based collision detection system. In: IEEE International Conference on Robotics and Automation, 2004, vol. 5, pp. 5212–5217 (2004). IEEE
7. Vidussi, F., Boscariol, P., Scalera, L., Gasparetto, A.: Local and trajectory-based indexes for task-related energetic performance optimization of robotic manipulators. J. Mech. Robot. **13**(2), 021018 (2021)
8. Fabris, G., Scalera, L., Gasparetto, A.: Dynamic modelling and energy-efficiency optimization in a 3-DOF parallel robot. Int. J. Adv. Manuf. Technol. **132**(5), 2677–2699 (2024)
9. Balderas Hill, R., Briot, S., Chriette, A., Martinet, P.: Minimizing the energy consumption of a Delta robot by exploiting the natural dynamics. In: ROMANSY 23-Robot Design, Dynamics and Control: Proceedings of the 23rd CISM IFToMM Symposium 23, pp. 213–221 (2021). Springer
10. Boscariol, P., Richiedei, D.: Energy-efficient design of multipoint trajectories for Cartesian robots. Int. J. Adv. Manuf. Technol. **102**, 1853–1870 (2019)
11. Van Oosterwyck, N., Vanbecelaere, F., Knaepkens, F., Monte, M., Stockman, K., Cuyt, A., Derammelaere, S.: Energy optimal point-to-point motion profile optimization. Mechanics Based Design of Structures and Machines, 1–18 (2022)
12. Fabris, G., Scalera, L., Gasparetto, A.: Online optimization and trajectory planning for energy efficiency in a robotic linear axis. In: Quaglia, G., Boschetti, G., Carbone, G. (eds.) Advances in Italian Mechanism Science. IFToMM Italy 2024. Mech. Mach. Sci., vol. 164, pp. 155–162 (2024). Springer, Cham
13. Márton, L., van der Linden, F.: Temperature dependent friction estimation: Application to lubricant health monitoring. Mechatronics **22**(8), 1078–1084 (2012)
14. Wang, J., Dong, X., Barry, O.R., Okwudire, C.: Friction-induced instability and vibration in a precision motion stage with a friction isolator. J. Vib. Control **28**(15–16), 1879–1893 (2022)
15. Dong, F., He, J., Zhao, X., Han, J., Huang, X., Zhang, X.: Analytical modeling method for joint friction in harmonic drive robot. J. Mech. Sci. Technol., 1–11 (2024)
16. Wu, J., Li, W., Xiong, Z.: Identification of robot dynamic model and joint frictions using a baseplate force sensor. SCIENCE CHINA Technol. Sci. **65**(1), 30–40 (2022)
17. Wahrburg, A., Klose, S., Clever, D., Groth, T., Moberg, S., Styrud, J., Ding, H.: Modeling speed-, load-, and position-dependent friction effects in strain wave gears. In: 2018 IEEE International Conference on Robotics and Automation (ICRA), pp. 2095–2102 (2018). IEEE
18. Harmonic Drive strain wave gear. https://harmonicdrive.de/en/glossary/harmonic-driver-strain-wave-gear. Accessed 10 July 2024 (2024)
19. Gravagno, F., Mucino, V.H., Pennestrì, E.: The mechanical efficiency of harmonic drives: A simplified model. J. Mech. Des. **143**(6), 063302 (2021)
20. Raviola, A., Guida, R., De Martin, A., Pastorelli, S., Mauro, S., Sorli, M.: Effects of temperature and mounting configuration on the dynamic parameters identification of industrial robots. Robotics **10**(3), 83 (2021)
21. Bittencourt, A.C., Gunnarsson, S.: Static Friction in a Robot Joint—Modeling and Identification of Load and Temperature Effects. J. Dyn. Syst. Meas. Contr. **134**(5), 051013 (2012)
22. Gaz, C., Magrini, E., De Luca, A.: A model-based residual approach for human-robot collaboration during manual polishing operations. Mechatronics **55**, 234–247 (2018)
23. Gaz, C., Cognetti, M., Oliva, A., Giordano, P.R.o., De Luca, A.: Dynamic identification of the Franka Emika Panda robot with

retrieval of feasible parameters using penalty-based optimization. IEEE Robot. Auto. Lett. **4**(4), 4147–4154 (2019)
24. Jung, D., Do, H., Choi, T., Park, J., Cheong, J.: Robust parameter estimation of robot manipulators using torque separation technique. IEEE Access **9**, 150443–150458 (2021)
25. Tadese, M.A., Yumbla, F., Yi, J.-S., Lee, W., Park, J., Moon, H.: Passivity guaranteed dynamic friction model with temperature and load correction: Modeling and compensation for collaborative industrial robot. IEEE Access **9**, 71210–71221 (2021)
26. Tadese, M., Pico, N., Seo, S., Moon, H.: A Two-Step Method for Dynamic Parameter Identification of Indy7 Collaborative Robot Manipulator. Sensors **22**(24), 9708 (2022)
27. Nevmerzhitskiy, M.N., Notkin, B.S., Vara, A.V., Zmeu, K.V., et al.: Friction model of industrial robot joint with temperature correction by example of KUKA KR10. J. Robot. **2019** (2019)
28. Indri, M., Trapani, S.: Framework for static and dynamic friction identification for industrial manipulators. IEEE/ASME Trans. Mechatron. **25**(3), 1589–1599 (2020)
29. Fabris, G., Scalera, L., Boscariol, P., Gasparetto, A.: Experimental analysis and comparison of friction models applied to the UR5e robot. In: Lovasz, EC., Ceccarelli, M., Ciupe, V. (eds.) Mechanism Design for Robotics. MEDER 2024. Mech. Mach. Sci., vol. 166, pp. 125–133 (2024). Springer, Cham
30. Makkar, C., Dixon, W.E., Sawyer, W.G., Hu, G.: A new continuously differentiable friction model for control systems design. In: IEEE/ASME International Conference on Advanced Intelligent Mechatronics, pp. 600–605 (2005). IEEE
31. Marques, F., Flores, P., Pimenta Claro, J., Lankarani, H.M.: A survey and comparison of several friction force models for dynamic analysis of multibody mechanical systems. Nonlinear Dyn. **86**, 1407–1443 (2016)
32. Piatkowski, T.: Dahl and LuGre dynamic friction models—The analysis of selected properties. Mech. Mach. Theory **73**, 91–100 (2014)
33. Coulomb, C.A.: Essai sur une application des règles de maximis et minimis à quelques problèmes de statique relatifs à l'architecture. Mem. Div. Sav. Acad. (1776)
34. Afrough, M., Hanieh, A.A.: Identification of Dynamic Parameters and Friction Coefficients: of a Robot with Planar Serial Kinemtic Linkage. J. Intell. Robot. Syst. **94**, 3–13 (2019)
35. Grotjahn, M., Daemi, M., Heimann, B.: Friction and rigid body identification of robot dynamics. Int. J. Solids Struct. **38**(10–13), 1889–1902 (2001)
36. Dong, J., Xu, J., Zhou, Q., Zhu, J., Yu, L.: Dynamic identification of industrial robot based on nonlinear friction model and LS-SOS algorithm. IEEE Trans. Instrum. Meas. **70**, 1–12 (2021)
37. Karahan, O., Karci, H.: Swarm intelligence based nonlinear friction and dynamic parameters identification for a 6-DOF robotic manipulator. J. Intell. Robot. Syst. **108**(2), 19 (2023)
38. Hao, L., Pagani, R., Beschi, M., Legnani, G.: Dynamic and friction parameters of an industrial robot: Identification, comparison and repetitiveness analysis. Robotics **10**(1), 49 (2021)
39. Wolf, S., Iskandar, M.: Extending a dynamic friction model with nonlinear viscous and thermal dependency for a motor and harmonic drive gear. In: 2018 IEEE International Conference on Robotics and Automation (ICRA), pp. 783–790 (2018). IEEE
40. Zhou, Y., Li, Z., Zhang, X., Li, Y., Zhu, M.: A Semi-linearized Approach for Dynamic Identification of Manipulator Based on Nonlinear Friction Model. IEEE Trans. Instrument. Measure. (2024)
41. Pennestrì, E., Rossi, V., Salvini, P., Valentini, P.P.: Review and comparison of dry friction force models. Nonlinear Dyn. **83**, 1785–1801 (2016)
42. Shao, X., Xie, L., Li, C., Li, Y.: Robot dynamics modeling with a novel friction model and extracted feasible parameters using constrained differential evolution. J. Intell. Robot. Syst. **108**(1), 5 (2023)
43. Indri, M., Lazzero, I., Antoniazza, A., Bottero, A.M.: Friction modeling and identification for industrial manipulators. In: 18th Conference on Emerging Technologies & Factory Automation, pp. 1–8 (2013). IEEE
44. Clochiatti, E., Scalera, L., Boscariol, P., Gasparetto, A.: Electromechanical modeling and identification of the UR5 e-series robot. Robotica **47**(7), 2430–2452 (2024)
45. Xiao, J., Zhang, Q., Hong, Y., Wang, G., Zeng, F.: Collision detection algorithm for collaborative robots considering joint friction. Int. J. Adv. Rob. Syst. **15**(4), 1729881418788992 (2018)
46. Gao, L., Yuan, J., Qian, Y.: Torque control based direct teaching for industrial robot considering temperature-load effects on joint friction. Industrial Robot: The International Journal of Robotics Research and Application **46**(5), 699–710 (2019)
47. Baur, J., Dendorfer, S., Pfaff, J., Schütz, C., Buschmann, T., Ulbrich, H.: Experimental friction identification in robot drives. In: 2014 IEEE International Conference on Robotics and Automation (ICRA), pp. 6006–6011 (2014). IEEE
48. Albu-Schaffer, A., Hirzinger, G.: Parameter identification and passivity based joint control for a 7 DOF torque controlled light weight robot. In: Proceedings 2001 ICRA. IEEE International Conference on Robotics and Automation (Cat. No. 01CH37164), vol. 3, pp. 2852–2858 (2001). IEEE
49. Hassen, M.D., Laamiri, I., Messaoud, H.: Exoskeleton Dynamic Modeling and Identification with Load and Temperature-Dependent Friction Model. In: 2021 IEEE 2nd International Conference on Signal, Control and Communication (SCC), pp. 14–19 (2021). IEEE
50. Li, Z., Wei, H., Liu, C., He, Y., Liu, G., Zhang, H., Li, W.: An improved iterative approach with a comprehensive friction model for identifying dynamic parameters of collaborative robots. Robotica **42**(5), 1500–1522 (2024)
51. Simoni, L., Beschi, M., Legnani, G., Visioli, A.: Modelling the temperature in joint friction of industrial manipulators. Robotica **37**(5), 906–927 (2019)
52. Iskandar, M., Wolf, S.: Dynamic friction model with thermal and load dependency: modeling, compensation, and external force estimation. In: 2019 International Conference on Robotics and Automation (ICRA), pp. 7367–7373 (2019). IEEE
53. Xiao, J., Dou, S., Zhao, W., Liu, H.: Sensorless human-robot collaborative assembly considering load and friction compensation. IEEE Robot. Auto. Lett. **6**(3), 5945–5952 (2021)
54. Keck, A., Zimmermann, J., Sawodny, O.: Friction parameter identification and compensation using the elastoplastic friction model. Mechatronics **47**, 168–182 (2017)
55. Dahl, P.R.: A solid friction model. El Segundo, CA, USA, Technical report. Aerospace Corp El Segundo Ca (1968)
56. Bliman, P.-A.: Friction modelling by hysteresis operators: application to Dahl, sticktion and Stribeck effects. In: Proceedings of the Conference on Models of Hysteresis, Trento, 1991 (1991)
57. Bliman, P.-A., Sorine, M.: A system-theoretic approach of systems with hysteresis. application to friction modelling and compensation. In: Proceedings of the 2nd European Control Conference, pp. 1844–1849 (1993)
58. Bliman, P.-A., Sorine, M.: Easy-to-use realistic dry friction models for automatic control. In: Proceedings of 3rd European Control Conference, vol. 113, pp. 267–272 (1995). Rome, Italy
59. Gafvert, M.: Comparisons of two dynamic friction models. In: Proceedings of the 1997 IEEE International Conference on Control Applications, pp. 386–391 (1997). IEEE
60. De Wit, C.C., Olsson, H., Astrom, K.J., Lischinsky, P.: A new model for control of systems with friction. IEEE Trans. Autom. Control **40**(3), 419–425 (1995)

61. Dupont, P., Armstrong, B., Hayward, V.: Elasto-plastic friction model: contact compliance and stiction. In: Proceedings of the 2000 American Control Conference. ACC (IEEE Cat. No. 00CH36334), vol. 2, pp. 1072–1077 (2000). IEEE
62. Swevers, J., Al-Bender, F., Ganseman, C.G., Projogo, T.: An integrated friction model structure with improved presliding behavior for accurate friction compensation. IEEE Trans. Autom. Control **45**(4), 675–686 (2000)
63. Lampaert, V., Al-Bender, F., Swevers, J.: A generalized Maxwell-slip friction model appropriate for control purposes. In: 2003 IEEE International Workshop on Workload Characterization (IEEE Cat. No. 03EX775), vol. 4, pp. 1170–1177 (2003). IEEE
64. Scalera, L., Nainer, C., Giusti, A., Gasparetto, A.: Robust safety zones for manipulators with uncertain dynamics in collaborative robotics. Int. J. Comput. Integr. Manuf. **37**(7), 887–899 (2024)
65. Park, J.: Motion profile planning of repetitive point-to-point control for maximum energy conversion efficiency under acceleration conditions. Mechatronics **6**(6), 649–663 (1996)
66. Harmonic Drive SE. https://harmonicdrive.de/en/product/gears-with-output-bearing/hfus-2uh-2so-2sh. Accessed 4 July 2024 (2024)
67. UR5e User Manual. https://s3-eu-west-1.amazonaws.com/ur-support-site/68265/99455_UR5e_User_Manual_en_US.pdf. Accessed 2 July 2024 (2024)
68. Tjahjowidodo, T., Al-Bender, F., Van Brussel, H.: Theoretical modelling and experimental identification of nonlinear torsional behaviour in harmonic drives. Mechatronics **23**(5), 497–504 (2013)
69. Cılız, M.K., Tomizuka, M.: Friction modelling and compensation for motion control using hybrid neural network models. Eng. Appl. Artif. Intell. **20**(7), 898–911 (2007)
70. Liu, S., Wang, L., Wang, X.V.: Sensorless force estimation for industrial robots using disturbance observer and neural learning of friction approximation. Robot. Comput.-Integr. Manuf. **71**, 102168 (2021)
71. Guo, K., Pan, Y., Yu, H.: Composite learning robot control with friction compensation: A neural network-based approach. IEEE Trans. Industr. Electron. **66**(10), 7841–7851 (2018)
72. Liu, X., Zhao, F., Ge, S.S., Wu, Y., Mei, X.: End-effector force estimation for flexible-joint robots with global friction approximation using neural networks. IEEE Trans. Industr. Inf. **15**(3), 1730–1741 (2018)
73. Scholl, P., Iskandar, M., Wolf, S., Lee, J., Bacho, A., Dietrich, A., Albu-Schäffer, A., Kutyniok, G.: Learning-based adaption of robotic friction models. Robot. Comput.-Integr. Manuf. **89**, 102780 (2024)

Giuliano Fabris studied Mechanical Engineering at the University of Udine (Italy), received his Bachelor's Degree in 2020, and his Master's Degree in 2023, both cum laude. From 2023 to 2024, he was a research fellow at University of Udine within the Interconnected Nord-Est Innovation Ecosystem (iNEST) project. Since 2024, he is working at the University of Udine as PhD student in Industrial and Information Engineering. In 2026 he was a visiting Ph.D. student at the Chiang Mai University (Thailand). His research interests are in the fields of collaborative robotics, dynamic modelling and trajectory planning for energy efficiency for mechatronic and robotic systems.

Lorenzo Scalera achieved the Master's degree in Mechanical Engineering (cum laude) at University of Trieste in 2015, and the Ph.D. in Industrial and Information Engineering at University of Udine (Italy) in 2019. In 2018 he was a visiting Ph.D. student at the Stevens Institute of Technology in Hoboken (NJ, USA). In 2019 he was a Post Doc Research Fellow at Free University of Bozen-Bolzano (Italy). From 2020 to 2024 he was Assistant Professor of Mechanics of Machines at the Polytechnic Department of Engineering and Architecture of the University of Udine. Since 2024 he is Associate Professor at University of Udine. He currently serves in the Editorial Board of IEEE Robotics and Automation Letters. He is author of more than 100 international publications in scientific journals and conferences. His research interests include dynamic modelling of mechatronic and robotic systems, trajectory planning, and collaborative robotics.

Paolo Boscariol achieved the Master's Degree in Electronic Engineering at the University of Udine in 2008, and the Ph.D. in Industrial and Information Engineering at the DIEGM, University of Udine, in 2021. Since 2016, he has been with the Department of Management and Engineering (DTG) at the University of Padova (Italy), where he has served as an Associate Professor since 2021. His research interests include motion planning for energy efficiency in robots and multibody systems, dynamic modeling of mechatronic systems, development of robust model-based motion planning algorithms for underactuated systems.

Alessandro Gasparetto received the MSc in Electronic Engineering from the University of Padova, Italy, in 1992; the MSc in Mathematics from University of Padova, Italy, in 2003; the PhD in Mechanics of Machines from University of Brescia, Italy, in 1996. He is Full Professor of Mechanics of Machines at the Polytechnic Department of Engineering and Architecture, University of Udine (Udine, Italy), where he is the head of the research group in Mechatronics and Robotics, as well as the Head of the Department (since 2021). Since 2019, he has been included in the the ranking of the top 2% most quoted and authoritative scientists in the world, published by researchers at Stanford University. From 2017 to 2023, he has been the Chair of IFToMM Italy, the Italian branch of IFToMM (the International Federation for the Promotion of Mechanism and Machine Science). From 2018 to 2023, he has been the Chair of the IFToMM Permenent Commission for the History of Mechanism and Machine Science. His research interests are in the fields of: modeling and control of mechatronic systems, robotics, mechanical design, industrial automation, mechanical vibrations. He is author of more than 200 international publications, and has been involved in the scientific and organizing committees of several conferences, as well as in many research projects, at the regional, national and European level.